



APPLICATION OF PRODUCTION DECLINE CURVE ANALYSIS TO CLASTIC RESERVOIR FACIES CHARACTERIZATION WITHIN A SEQUENCE STRATIGRAPHIC FRAMEWORK: EXAMPLE—FRIO FORMATION, SOUTH TEXAS

John D. Pigott¹ and Bryant W. Bradley^{1,2}

¹*ConocoPhillips School of Geology and Geophysics, University of Oklahoma, Sarkeys Energy Center, Ste. 710, 100 E. Boyd St., Norman, Oklahoma 73019, U.S.A.*

²*Chevron North America Exploration & Production, 1500 Louisiana St., Houston, Texas 77002, U.S.A.*

ABSTRACT

Viewed within a dynamic 3D accommodation perspective, petrophysical log motifs of 113 wells in the adjoining Captain Lucey and Richard King fields of Jim Wells and Nueces counties, South Texas, reveal the overprint of fourth-order autocyclic processes of regression and transgression within a general third-order allocyclic sea level fall. Five reservoir sand environmental assemblages sealed by transgressive systems tract (TST) shales identified within the clastic shelf wedge of the Oligocene-Miocene Frio Formation are: lowstand systems tract (LST) delta 1, regressive systems tract (RST) to LST delta plain distributaries, RST–LST distributary crevasse splay, TST barrier island, and LST–RST delta 2.

Production decline curve analysis (PDCA) of 18 reservoirs in 12 of 20 currently active wells of these two fields demonstrate a systematic relationship between reservoir elements and their associated depositional environments. The deltaic 1 and deltaic 2 environments (delta front sands) have the best reservoir quality sands of the five, exhibiting linear lowest decline rates with the highest average flow permeabilities (80 md) and largest drainage areas (290 ac). A close second in drainage area (251 ac) is the barrier island sand with lower average flow permeability (7 md). The fluvial sand exhibits the highest decline rates with good drainage area (214 ac) and modest average permeability (32 md). The poorest reservoir quality is the crevasse splay sand with rapidly declining rates, lowest average permeability (0.8 md) and smallest drainage area (110 ac).

The strong relationships between PDCA and depositional environments in these South Texas Frio Formation sands point to the potential applicability of PDCA—depositional facies linkages as a reservoir performance predictor in fields elsewhere.

INTRODUCTION: PROBLEM DEFINITION

For coastal depositional systems, when examining vertical facies relationships which are sensitive both to bathymetry and to lateral changes in process energy, two unanswered questions often arise when interpreting high energy deposits transitionally overlying low energy deposits or conversely, low energy deposits transitionally overlying high energy deposits: Is the shoaling upward package indicative of a simple regression (caused by increased sediment influx) or a forced regression (caused by a sea level fall)? Or, is the deepening upward package a simple trans-

gression (caused by decreased sediment influx) or a forced transgression (one caused by sea level rise)? One may phrase the two ends of the spectrum of process-response question in yet another way: Is the process responsible for the observed facies vertical succession a product of autocyclic (intra-basinal) or allocyclic (extra-basinal) processes? That is, as an operational example, if one is employing wireline logs, how does one separate autocyclic (intra-basinal) from allocyclic (extra-basinal) changes in process-response? Attempting to answer such questions from an accommodation perspective can provide significant exploration insight into the delineation of regional exploration fairways, and moreover can augment information concerning exploitation strategies of existing fields. There is a third question that only a mature field can answer. Production decline curve analysis (PDCA) for producing oil and gas fields is a classic method for examining well performance, forecasting future production, and determining value of the producing asset. This study asks: Can PDCA addi-

Copyright © 2014. Gulf Coast Association of Geological Societies. All rights reserved.

Manuscript received March 31, 2014; revised manuscript received July 3, 2014; manuscript accepted July 10, 2014.

GCAGS Journal, v. 3 (2014), p. 111–134.

tionally provide geologically useful insight into reservoir facies and associated reservoir qualities? This paper will attempt to answer these three questions for the fluvial deltaic depositional systems of the Frio Formation of the mature Captain Lucey and Richard King fields of South Texas (Fig. 1), an ideal laboratory for such an investigation.

REGIONAL SETTING

Stratigraphy

The Oligocene-Miocene sedimentary record on the northern margin of the Gulf Coast of Texas corresponds to a third-order global sea level cycle and a half (Fig. 2) made up of three limbs. The cycle commences with a Rupellian global sea level rise, is followed by a Chattian sea level fall, and culminates in an Aquitanian global sea level rise. The Rupellian rising sea level phase is recorded by the Vicksburg Formation and several thousand ft of undercompacted slope and basinal mudstone deposits. The ensuing Chattian falling sea level phase is recorded by the onset of overlying Frio Formation sedimentation (Fig. 2). Termed the Frio wedge major stratigraphic unit (Holtz and McRae, 1995), these sediments are characterized as stacked fluvial-deltaic deposits associated with significant extensional faulting (Galloway et al., 1982). The subsequent Aquitanian rise in global sea level (Fig. 2) is recorded in South Texas by the deposition of the trans-

gressive, marine Anahuac Shale (Lawless et al., 1997) with the *Heterostegina* Zone, a micropaleontologic marker zone (Akers and Drooger, 1957). The Chattian to Aquitanian Frio Formation, a major Tertiary hydrocarbon reservoir producer on the Gulf of Mexico Coastal Plain, forms the stratigraphic focus of this paper. Operationally, the Frio within the study area is subdivided and correlated not by micropaleontological evidence, but lithostratigraphically by local wireline log pattern similarities.

Structure

The Gulf Coast Tertiary Basin is characterized as an extra-cratonic (passive margin) basin that formed under conditions of rapid subsidence accompanying intense sediment loading (Galloway et al., 1982). Lying within is the Rio Grande embayment, a structural province characterized by discontinuous belts of growth faults and deep-seated shale ridges and massifs. Increased sediment loading, owing to the deposition of the Frio wedge, contributed to regional instability. The rapid loading of water-saturated shales downsection of the Frio and at the crest of a gently inclined subaqueous slope resulted in regional, syndepositional down-to-the-coast faulting and intrastratal deformation (Galloway et al., 1982). Two primary fault zones, the Vicksburg Flexure and Frio Fault Zone, are the direct result of this rapid early Oligocene sediment loading.

Figure 1. Location of the 113 wells of Captain Lucey and Richard King fields in Jim Wells and Nueces counties of South Texas.

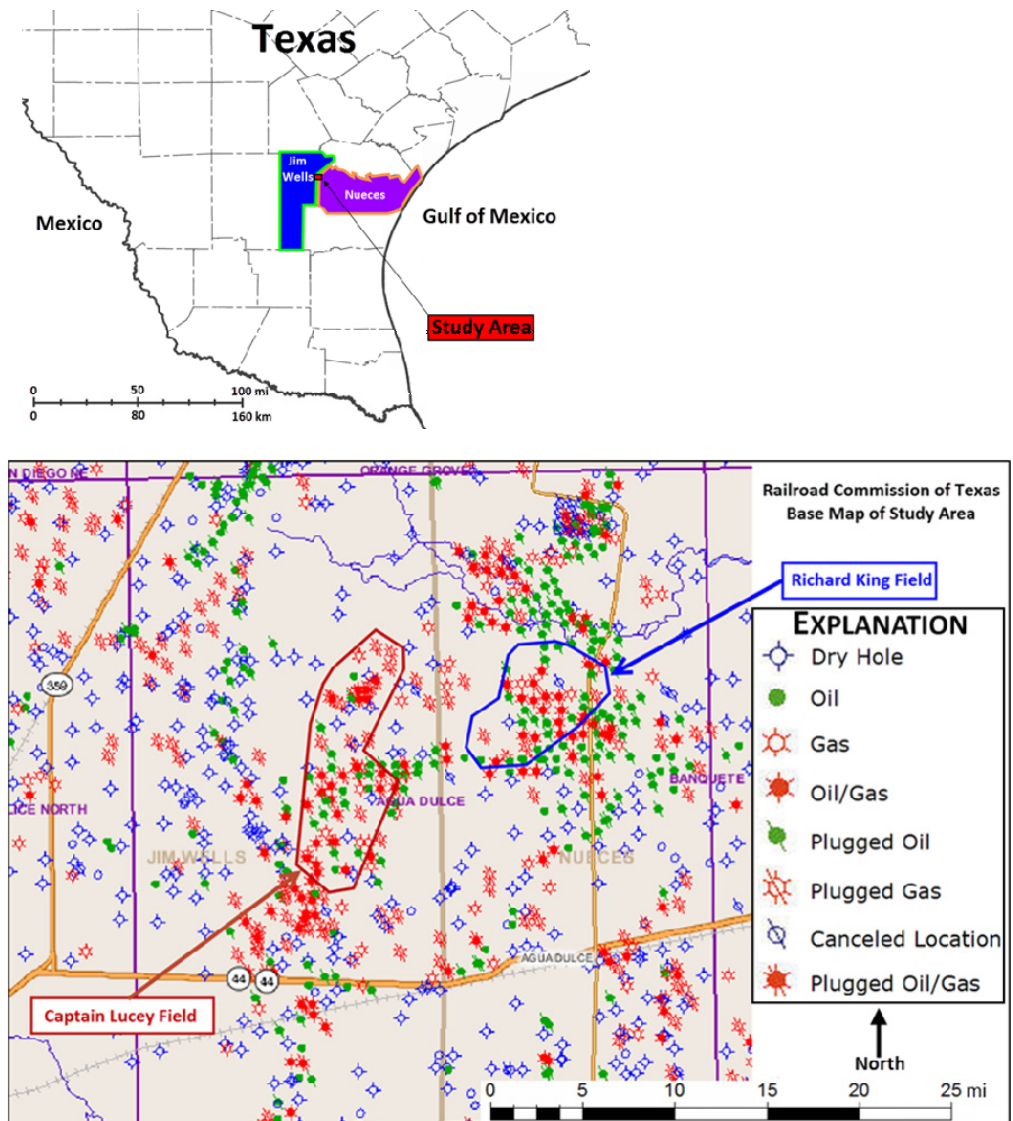


Figure 1. Location of the 113 wells of Captain Lucey and Richard King fields in Jim Wells and Nueces counties of South Texas.

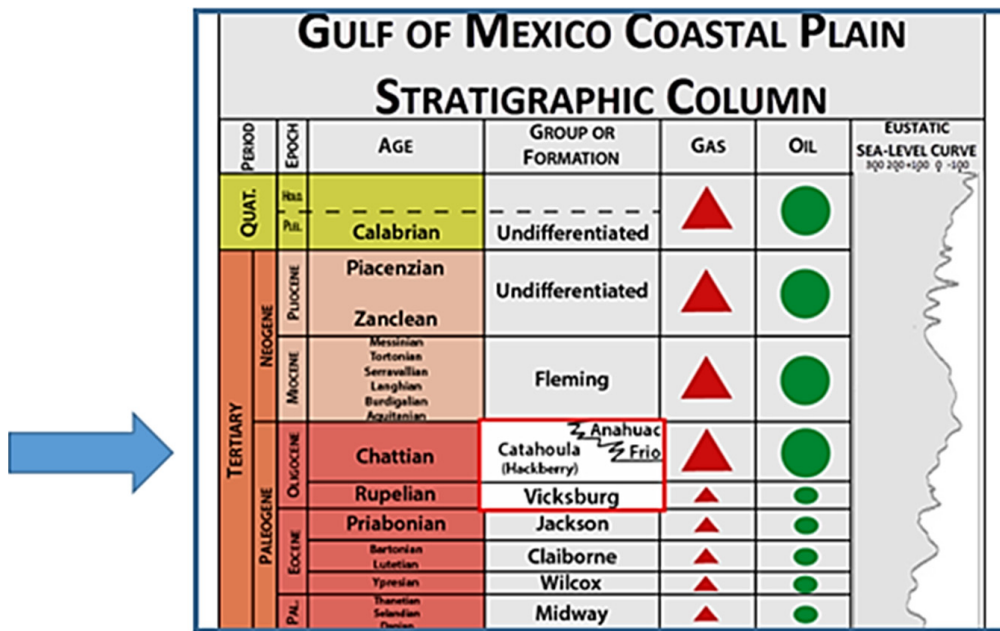


Figure 2. Stratigraphic column of the Gulf of Mexico Coastal Plain showing major oil and gas producing units juxtaposed with the eustatic sea-level curve (modified after Swanson et al., 2007; Haq and Al-Qahtani, 2005). Gas (red triangle) and oil (green circle) columns refer to regionally producing reservoirs. Frio deposition (indicated by the blue arrow) occurred during a Chattian second-order global sea level fall with three minor apexes of third-order high sea levels, which give way to a third-order Aquitanian sea level rise.

The Vicksburg Flexure, a narrow fault zone characterized by intense vertical displacement of older strata, provides a boundary of significant structural deformation within the updip portion of the Frio. For the study area (Fig. 3), it is the Frio Fault Zone that developed downdip of the Vicksburg Flexure during the early to middle Oligocene that controls the local structuring. This flexure is characterized by broad, deep listric normal faults and associated rollover anticlines (Swanson et al., 2007).

Depositional Systems

Four major ancient progradational complexes, the Central Mississippi, Houston, Norias, and Norma delta systems, are responsible for Frio sediment deposition in the Texas Gulf Coast Basin. Of these four, it is the Norias delta system of the study area which is a combination of wave-modified, lobate to wave-dominated, cusped deltas. Primary facies assemblages include delta-plain, delta-front, and delta-flank sandstones and mudstones, and underlying prodelta and upper slope mudstones (Galloway et al., 1982). The Norias was a laterally expansive, predominantly sandy, progradational delta system that allowed for deposition and filling of the Rio Grande Embayment. Progradation of the Norias delta system commenced during an early sea level rise (Duncan, 1983). As sea level rose, the Gueydan fluvial system of the Rio Grande Embayment (Galloway et al., 1982) deflected northward occupying a topographically low expression of the underlying Vicksburg progradational wedge. Subsequently, the Norias delta system became established as a stable progradational depositional system located laterally to the northward flanking margin of the main Vicksburg deltaic platform. The Norias is subdivided into three discrete genetically-related time equivalent units (Duncan, 1983) of which the middle unit represents Frio deposition in the study area. This middle unit evolved into a lobate, fluvial to wave-dominated, constructive delta system best characterized by the northern development of strandplain and barrier systems, termed the Greta barrier island system (Galloway et al., 1982).

DATA

Core, Petrophysical, and Production Information

The data for this study included detailed core analysis, historical production data, and petrophysical logs for wells within

the Captain Lucey (Jim Wells County, Texas) and Richard King (Nueces County, Texas) fields (Fig. 4). The Captain Lucey Field contains 15 currently active wells and the Richard King Field contains 5 currently active wells. This field study area covers an approximately 30 sq. mi block of these two counties and encompasses approximately 19,200 ac.

Detailed percussion sidewall core analysis of reservoir sands from 29 completed wells were used in this field study. Typical detailed core analysis included permeability, porosity, residual saturation percentage of pore space (oil and total water), residual saturation percentage of volume (oil and gas), lithological description, probable production (oil, gas, condensate, and water), API (American Petroleum Institute) gravity units, gas detection units, odor, and fluorescence. The level of analysis of the 29 cores varied in detail and completeness.

The production data for approximately 475 wells and electric log data from approximately 113 wells (Fig. 1) were provided by the operator, Quatro Oil & Gas. Production data, including current and historical production trends, were accessed for individual active and inactive wells located within the parameters of this field study through Lasser Production Data (LPD) software. Electric well log analysis was performed using IHS Petra and Schlumberger's Petrel geologic software packages, as well as Schlumberger's Techlog64 petrophysical software package.

FIELD PRODUCTION HISTORY

Captain Lucey Field

The discovery well in the Captain Lucey Field was the "No. 2 Bowers," announced April 16, 1939, by Damascus Corporation of San Antonio, Texas. The Captain Lucey Field (Jim Wells County, Texas) is one of several multi-reservoir fields that form the fluvial-deltaic sandstone gas play just east of the Vicksburg Flexure. It is located approximately 39 mi to the west of the city of Corpus Christi, Texas. Initial development of the Captain Lucey Field was limited to shallow gas reservoirs from the Upper and Middle Frio channel-fill deposits, where trapping occurred along the Vicksburg Fault. In the later stage of field development, oil and gas production was discovered in the stratigraphically lower reservoirs of the Lower Frio and Upper Vicksburg formations, with hydrocarbon entrapment in those reservoirs primarily related to the Vicksburg Fault. The Captain Lucey Field was developed with a 40-ac well spacing.

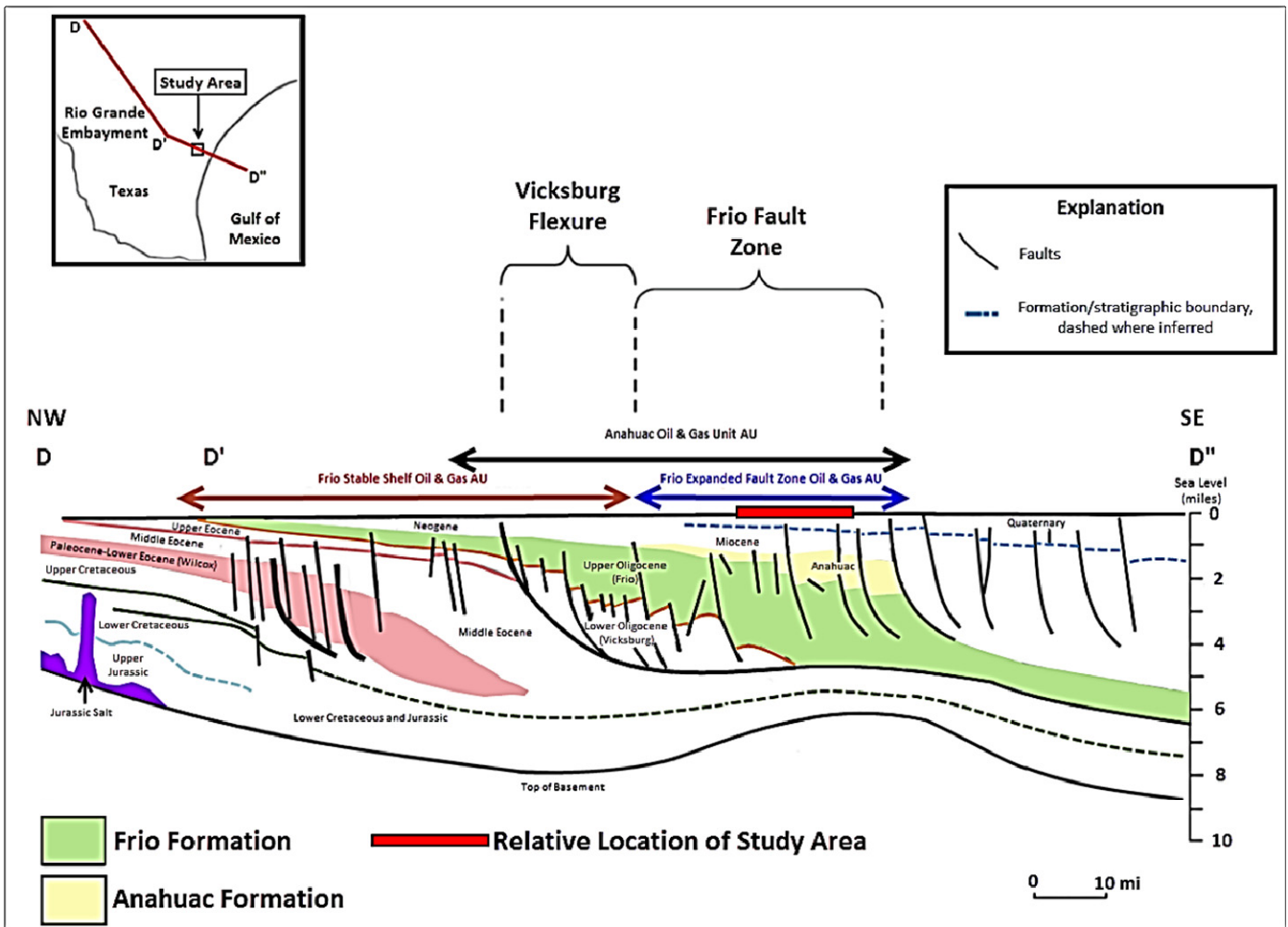
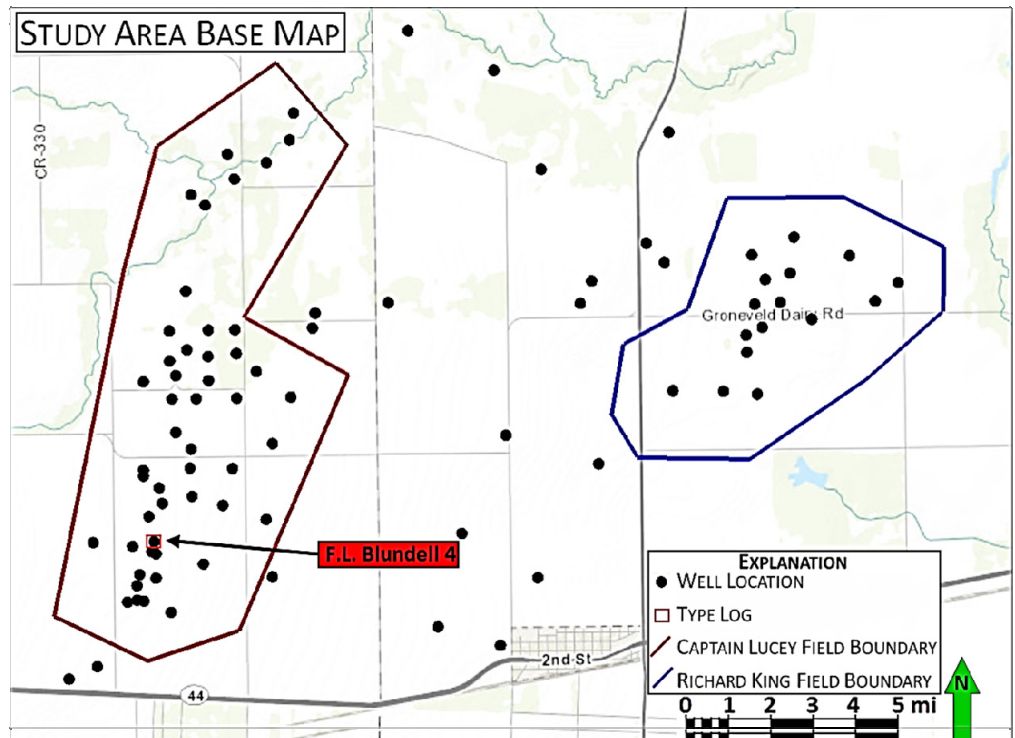


Figure 3. Regional northwest-southeast cross section of Central Texas illustrating the Early Cretaceous shelf margin extending to the present day shelf margin (modified after Swanson et al., 2007). The study area is indicated by the red horizontal line overlying the Frio Fault Zone, which occurs down-dip of the Vicksburg flexure (see text).

Figure 4. Base map of the study area. The Captain Lucey Field (Jim Wells County, Texas) is outlined by the red polygon. Immediately to its East is the Richard King Field (Nueces County, Texas) outlined by the blue polygon.



The Moore-Kimbrough #1 was drilled by Quatro in 1996 in order to test for potential trapping adjacent to inferred faulting on the eastern property limits of the Captain Lucey Field. Faulting was proven to exist with the discovery of three gas and two oil reservoirs, all of which possessed virgin reservoir pressure. Additionally, above the fault plane, two partially depleted gas reservoirs were identified. The producing reservoir of the Moore-Kimbrough #1 well was completed without stimulation at a depth of approximately 5000 ft. The Moore-Kimbrough #1 well currently produces 18 BOPD (barrels of oil per day) and 50 MCFGPD (thousand cubic ft of gas per day). The well has cumulatively produced approximately 58 MBO (thousand barrels of oil) and 331 MMCFG (million cubic ft of gas) from this reservoir with little decline in production. All other zones remain behind pipe in the Moore-Kimbrough #1 well.

The F. L. Blundell 4 well, which is also located in the Captain Lucey Field, will serve as the type well for the study area as

it is most representative of the area's generalized stratigraphy and reservoir properties (Fig. 5). Five of the most important stratigraphic tops are displayed on the type log based on their historical significance to hydrocarbon production. The F. L. Blundell 4 type log exemplifies the fluvial-deltaic nature of the Frio. As it is difficult within the study area to find multiple widespread, geologically extensive correlative stratigraphic marker beds, the "Het C" marker (top of the *Heterostegina* sp. carbonate-rich sandstone) is the only widespread correlative time-stratigraphic marker bed.

The F. L. Blundell 4 monthly production graph will serve as the type production curve for the study (Fig. 6). The F. L. Blundell 4 had cumulative production of 49 MBO and 55 MMCFG, and was eventually plugged and abandoned owing to mechanical failure. The cumulative production graph reveals the F. L. Blundell 4 gas production began to outpace oil production approximately midway through the life of the well (January 1, 1977), indicating the bubble point.

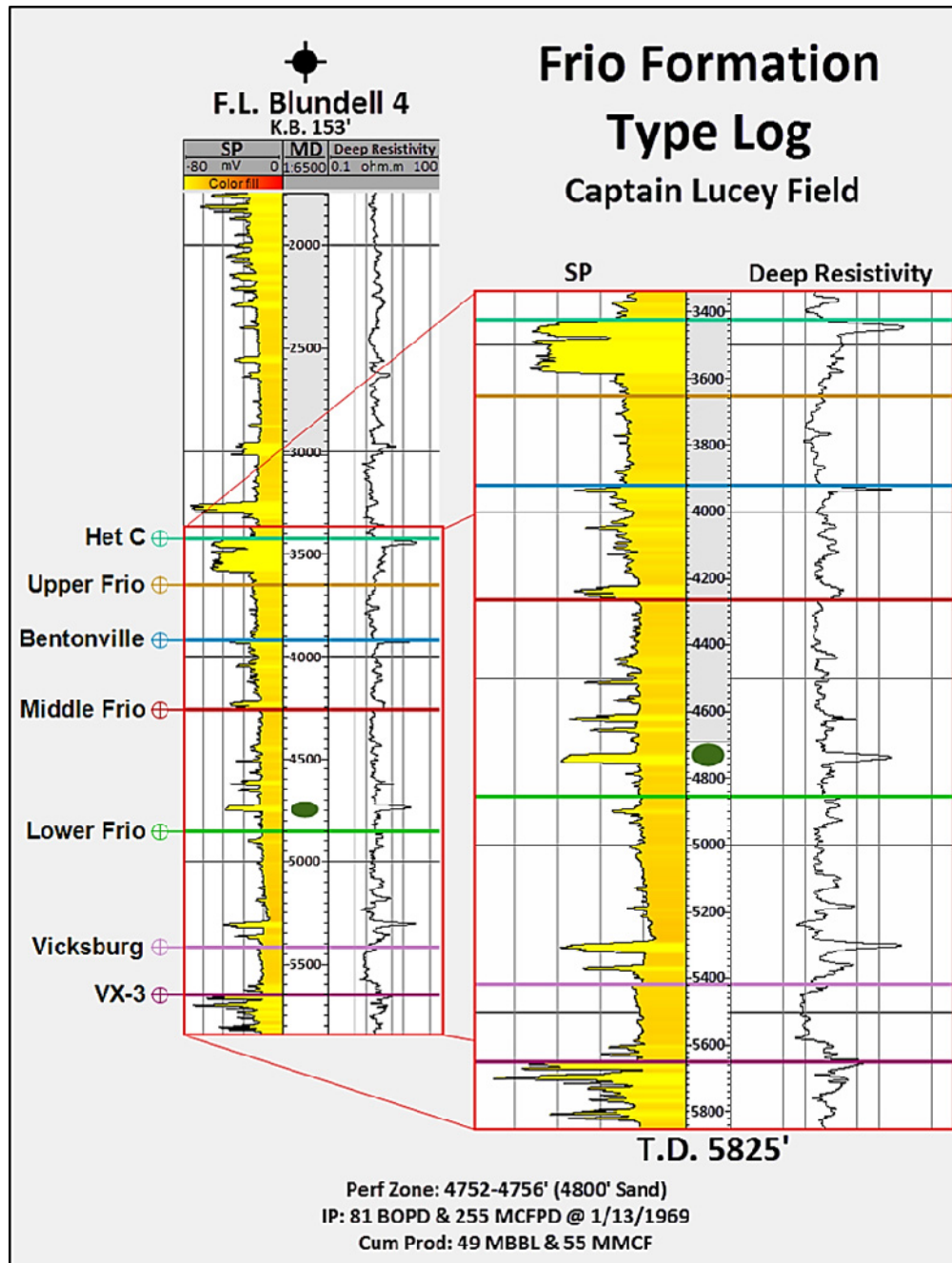


Figure 5. Type log for the F. L. Blundell 4 well with internal of interest enlarged. SP curve (track one) and deep resistivity curve (track two). Green ellipse indicates producing zone in this well. Note the numerous non-selected potential sands with high resistivities that were not selected indicating potentially by-passed pay (see text).

Type Production Curve: F.L. Blundell 4

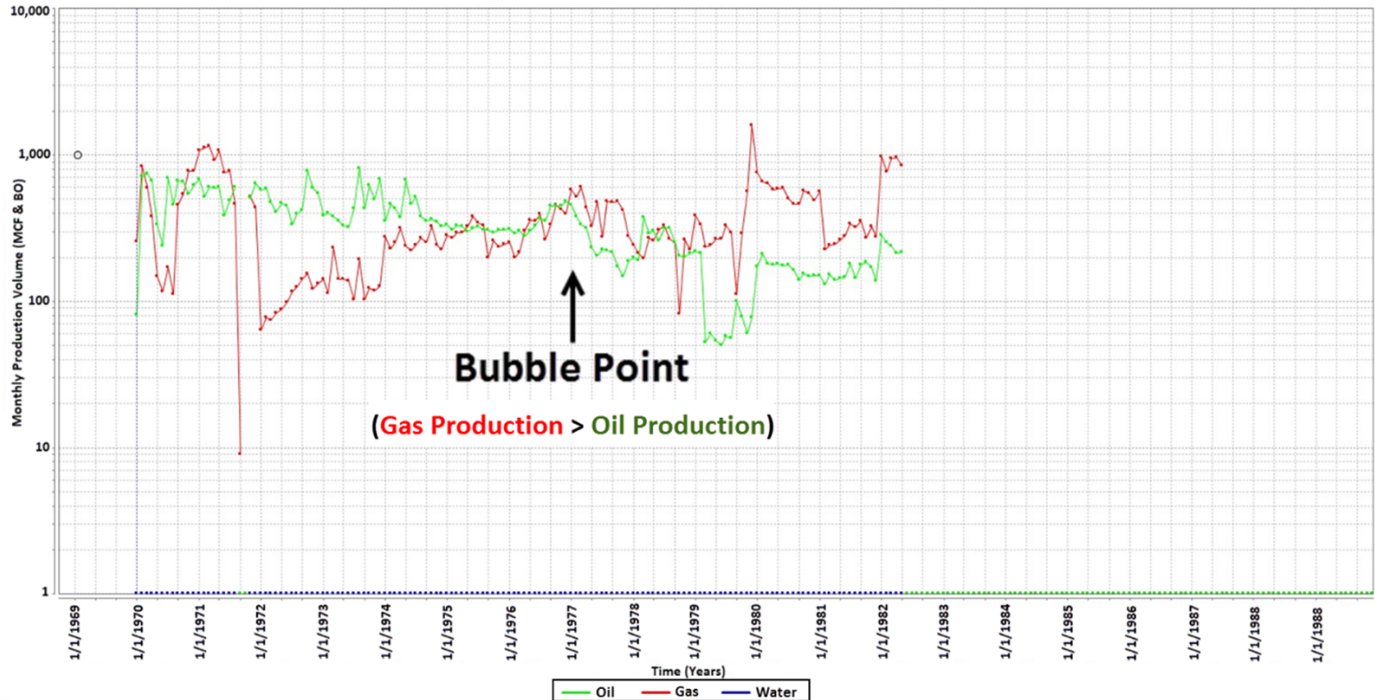


Figure 6. Type production curve (F. L. Blundell 4 well) for the study area. The bubble point is reached around January 1, 1977, where monthly production of gas begins to outpace monthly production of oil. Well was later plugged and abandoned owing to mechanical issues.

Approximately 55 wells were drilled from the late 1930s to late 1980s in the Captain Lucey Field. Over 85% of the cumulative oil and gas production was produced prior to 1980, after which the majority of wells drilled were deemed either dry-holes or non-commercial. Currently, 28 of the 55 wells in the Captain Lucey Field are plugged and abandoned. Cumulative production in the Captain Lucey Field is approximately 744.6 MBO and 5.6 BCFG (billion cubic ft of gas) (Fig. 7A) (Quatro, 2013, personal communication).

Richard King Field

The Richard King Field (Nueces County, Texas) is located approximately 5 mi to the northeast of the Captain Lucey Field and 29 mi to the west of Corpus Christi, Texas. This field is located within the Rio Grande Embayment, and similar to the Captain Lucey Field, which also may be characterized by its multi-reservoir nature resulting from its fluvial-deltaic depositional environment.

The initial discovery well in the Richard King Field, the Walker #1, was drilled in November of 1975 by the Frio Exploration Company of Houston, Texas. The Walker #1, was completed at a depth of approximately 5530 ft in a fault block on the southeastern flank of the Richard King Field. Hydrocarbon trapping in this reservoir was the result of antithetic faulting that occurred within the Frio Formation. The Walker #1 had an initial production of 100 BOPD and 225 MCFGPD with a cumulative production of 658 MBO and 493 MMCFG. The Richard King Field was developed with a 40-ac well spacing.

Approximately 27 wells were drilled in the Richard King Field from 1975 to 2013 with over 70% of cumulative production occurring prior to 1990. Cumulative production to the present in the Richard King Field amounts to approximately 1244 MBO (million barrels of oil) and 2.3 BCFG (Fig. 7B) (Quatro, 2013, personal communication).

ALLOCYCLIC AUTOCYCLIC PROCESS DIFFERENTIATION, 3D ACCOMMODATION, AND SEQUENCE STRATIGRAPHY

Theory

Alloyclic in the sense of Beerbower (1964) connotes processes that are principally extrabasinal, and for this paper are chiefly periodic and eustatic, but include external basinal architectural processes such as regional subsidence-uptift. Autocyclic connotes those processes that are chiefly intrabasinal, aperiodic, and chiefly sedimentologic but includes penecontemporaneous changes in intrabasinal architecture such as the growth and propagation of synsedimentary faulting. But herein lies the problem. Determining whether alloyclic or autocyclic processes are dominant can be challenging, as presently there exists an inherent interpretive bias of theory and tools utilized. This difficulty in their discrimination dates back to the very genetic sequence stratigraphic argument (see review by Christie-Blick and Driscoll, 1995) which accompanied the onset of the science of seismic sequence stratigraphy (Vail et al., 1977; Payton 1977), growing out of the concept of the sequence originated by Sloss (1963). This argument stemmed in part from the lack of agreement in selecting as of primary importance the basic boundary of sediment packages as being either alloyclic unconformities and their correlative conformities (Mitchum, 1977) or boundaries imposed by autocyclic intervals of sediment starvation (Galloway 1989). Arguments persist (e.g., Miall, 2010), as do continuing attempts of reconciliation (the *oeuvre* of Catuneanu, 2007) and his proposals for standardization (Catuneanu, 2009). However, for subsurface workers, the ongoing polemics and ever-increasing sequence stratigraphic vocabulary largely take a back-seat to the utilitarian necessity required by what particular tool is employed for stratigraphic interpretation: reflection seismic or wireline logs. As alloyclic unconformities commonly exhibit acoustic

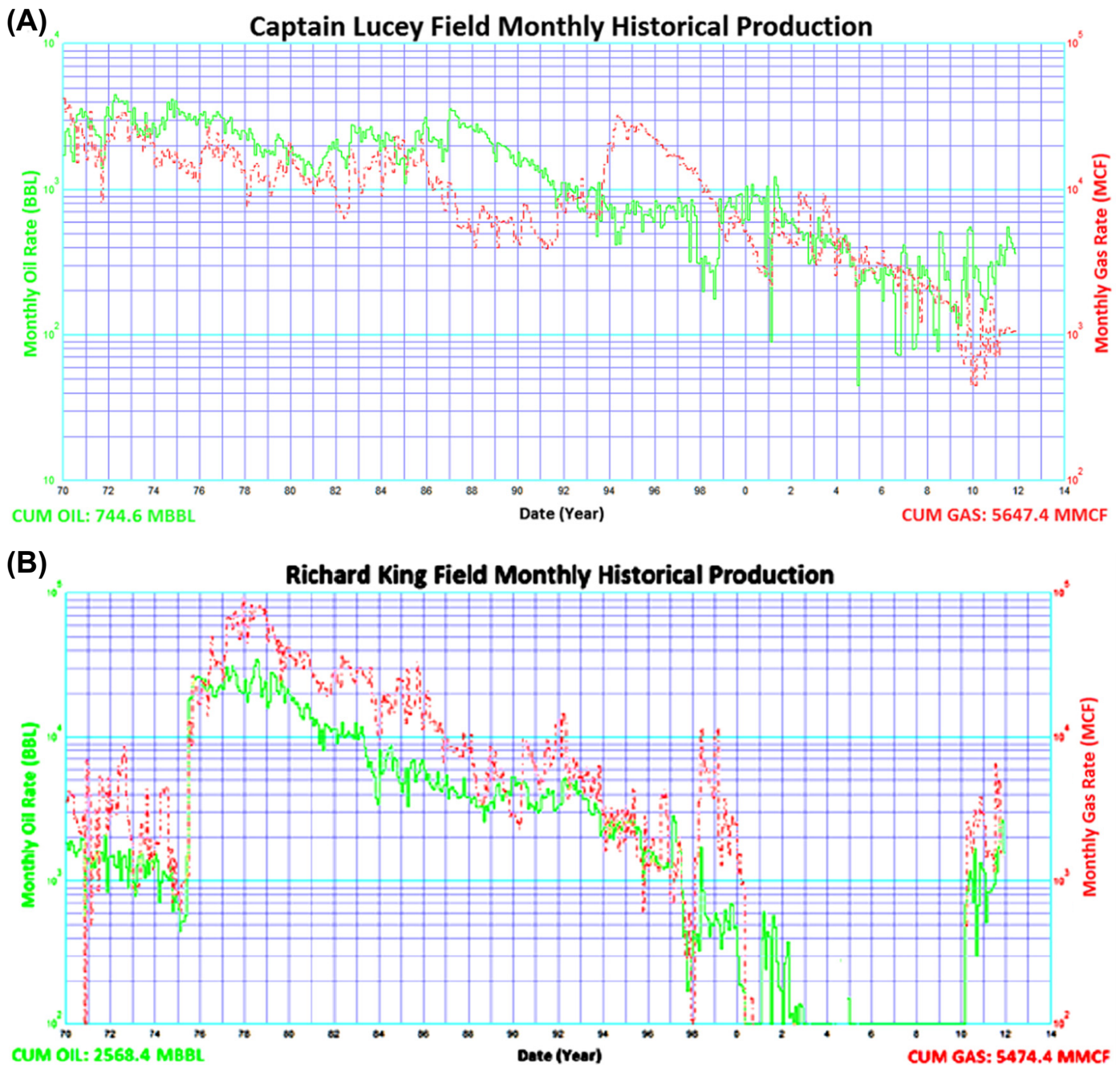


Figure 7. Historical production curve for the (a) Captain Lucey Field, all wells, and (b) Richard King Field, all wells. Green solid line indicates oil and red dashed line indicates gas.

impedance contrasts, such horizons are readily interpreted and correlated regionally by reflection seismic. As autocyclic flooding surfaces are commonly accompanied by the deposition of fine-grained deposits, these pronounced radioactive hot zones are locally readily identified and correlated on wireline logs.

If originating from a purely petrophysical assessment (e.g., gamma ray log, SP [spontaneous potential] log, etc.) that lacks a regional to global geometric time-equivalent perspective, the precise cause of sedimentologic responses to observed intrabasin vertical accommodation fill, removal, or datum stillstand would appear indeterminate. For example, is an observed regression of proximal, predominantly high energy deposits overlying distal, predominantly low energy deposits caused by an autocyclic overly abundant sediment supply during a stillstand, or is it a forced regression owing to an allocyclic sea level fall and marine

retreat across a low angled coastal plain? Conversely, is an observed transgression of distal, chiefly low energy deposits overlying proximal, chiefly high energy deposits the result of an autocyclic diminished sediment supply during a stillstand, or is it the result of an allocyclic sea level rise and a retreating or retrograding coastal depositional system? Finally, is an observed stationary shoreline with vertically stacked facies caused by an autocyclic sediment supply balanced by removal during an allocyclic stillstand in sea level, or is it a response to an accretion which is balanced by a relative sea level rise? If we incorporate the insight of the horizontal aspect afforded by the contributions of seismic stratigraphic models (e.g., Payton, 1977) with the contributions afforded in vertical motif interpretations provided by genetic stratigraphy (e.g., Galloway and Hobday, 1983) and integrate these perspectives by recognition of the three dimensional

perspective of accommodation fill and removal, then we can make progress in solving these questions. The discrimination of allocyclic and autocyclic controls upon accommodation fill-removal is critical in establishing the processes behind the observed hierarchical order of sequence stratigraphy and in subsequently constructing predictive models for local to regional characterizations of petroleum reservoirs, sources, and seals for exploration.

The key lies within the sedimentary record—its geometries, paleoenvironments, and time boundaries—that provides insight into the controlling local and regional processes responsible for its deposition. It is especially the geometry of sedimentary fill and removal that, if preserved, forms the most basic foundation for interpreting the interplay between allocyclic and autocyclic processes.

This geometric space potentially available for sediment accumulation is termed accommodation space (Wright and Marriott, 1993) or, more concisely as simply “accommodation” (Jervey, 1998). While Jervey argued that the major control upon accommodation was change in relative sea level and Catneanu (2007) among others argued that sedimentation rate was also important, one may take this definition out of the theoretical domain and into the pragmatic and operational domain in the following way. That is, the sedimentary record volume fill or removal is in a very real sense an *a posteriori*, observable record of the actual utilization of geometric space that was made available or unavailable for sediment accumulation. If accommodation is considered as the potential spatial volume for land-sea sediment accumulation with sea level as its upper boundary, with the underlying older sediments or rocks as the lower boundary and the lateral boundaries as indicated by baselap onlapping and downlapping time-physical surfaces, then it is useful to describe the response of sediments to dynamic change of this three dimensional space both vertically and horizontally as indicative of changes in allocyclic and autocyclic processes

Figure 8 illustrates six schematic process-response models for a variety of volume changes and resulting sedimentary geometries from the interplay between allocyclic and autocyclic processes and responses. These models will also have illustrative bearing upon the sequence discussion which follows. Commencing a cycle with the most basic model, Figure 8A illustrates an ensuing allocyclic still-stand in global sea level, such stasis in vertical accommodation accompanying an autocyclic sediment influx yields a decrease in the downdip horizontal accommodation. The product of this accommodation scenario is a toplapping and offlapping regression with horizontal basinward facies persistence of high energy deposits overlying lower energy deposits. Figure 8B illustrates a weak autocyclic dip fed fluvial system accompanying a strong allocyclic sea level rise. As both vertical and horizontal accommodation have increased, this dominantly allocyclic response is revealed by a forced transgression with the accretionary fill of coastal aggradation shown by system upstepping of low energy facies overlying high energy facies. In comparison, Figure 8C illustrates the effects of a strong autocyclic fluvial system following a waning allocyclic sea level rise which results in an increase in both vertical and horizontal accommodation. Here these partially disjunctive processes culminate in an offlapping regressive system similar to Figure 8A. Ending the cycle are Figures 8D and 8E. Figure 8D portrays a conjunctive allocyclic sea level fall with a strong autocyclic input which responds to the decrease in vertical accommodation by updip truncation of emerging underlying strata and forced regression system progradation causing a decrease in downdip horizontal accommodation. Figure 8E reveals an identical sedimentologic response as Figure 8D but with autocyclic basin uplift causing a relative sea level fall (indicated by the brown arrow). To complete these schematic process-response models of accommodation, Figure 8E presents the case for horizontal and vertical accommodation stasis. With balanced autocyclic input and remov-

al and no change in relative sea level, a stationary shoreline results.

Having established a schematic three dimensional geometric model of accommodation, it is instructive to compare this geometry to the expression of vertical changes in space from the portrayed conventional relative sea level curve and its associated parasquence sets. Relative sea level changes as indicated from the geometry of sediment record preservation or lack of preservation occur from a combination of the effects of subsidence, uplift, sediment supply and removal, thus an interplay between vertical allocyclic and horizontal autocyclic processes. Figure 9 is a schematic of a relative sea level curve for a complete cycle of sea level fall and rise and its associated clastic depositional systems. The falling limb on the relative sea level curve occurs during the interval in the cycle where vertical accommodation is decreasing, and the rising limb on the relative sea level curve occurs during the interval in the cycle where vertical accommodation is increasing. Assuming a coastal model of continuous fluvial clastic input, throughout the falling stage of relative sea level, termed the regressive systems tract (RST) (see review by Cantuneanu [2006] of Curray's [1964] original, but mis-positioned, RST terminology, and revised parasequence set positioning using fluvial examples by Pigott et al. [2012] and Pigott and Abdel-Fattah [2014], subaerial exposure of the shelf occurs, creating an unconformity or surface of nondeposition; slumps and mass transport complexes occur at the base of a sequence owing to the destabilization of the shelf margin during this time of decreasing vertical accommodation. Onshore the coastal plain, fluvial terraces form accompanying valley incision into the previously deposited highstand deposits. Sediments genetically linked at this time are deposited subaqueously either as downstepping deltas or off the shelf break as deep water submarine fans. Depending upon the magnitude of fall, as the relative rate of sea level fall decreases, sediment deposition occurs on the shelf as lowstand deltas or off the shelf as lowstand fans, sheets, lobes, and channel-levee complexes. This downstepping geometry of this falling stage is represented by Figures 8D and 8E. As relative sea level reaches the inflection point between the falling and rising limbs of one complete sea level cycle, sediment deposition occurs as channel fill, lowstand slope fans and early lowstand wedges. If during this stage of lowstand systems tracts (LST) development, a stasis between changes in vertical and horizontal accommodation occurs, a stationary shoreline (Fig. 8F) results. If instead sediment input is substantial, then progradation of sediments occurs with lateral accommodation decreasing (Fig. 8A). Following the inflection point of the sea level cycle, relative sea level rise increases rapidly, sediment deposition on the shelf and in incised valleys occurs first by way of basal fluvial deposits that grade into estuarine deposits as sea level rises (Fig. 8B). As the rate of relative sea level rise increases with an increase in vertical accommodation, barrier islands, lagoon, beach, and shoreface strata, and ebb-and-flood tidal deltas develop and become preserved. Accompanying the increase in lateral accommodation, the landward-stepping transgressive system tract is preserved beneath onlapping, low energy sediment fines. This stage of the transgressive systems tract (TST) is characterized by sediment deposition in both a retrogradational and aggradational style. It is typical for the deposition of mud to dominate in the distal marine environments at this time. As relative sea level rise reaches its maximum point during the TST, fine-grained, organic rich condensed sections may be deposited and are overlain by a maximum flooding surface (MFS). Owing in part to the drowning of clastic tributaries and point source flow and as deltas are now more widespread, a condensed section (CS) tends to blanket the shelf, slope, and basin, a key deposit identifiable as hot shales in well logs and commonly observed as laterally persistent bright amplitude reflectors on seismic. The MFS is representative of the maximum landward extent of the shoreline and maximum water depth on the shelf.

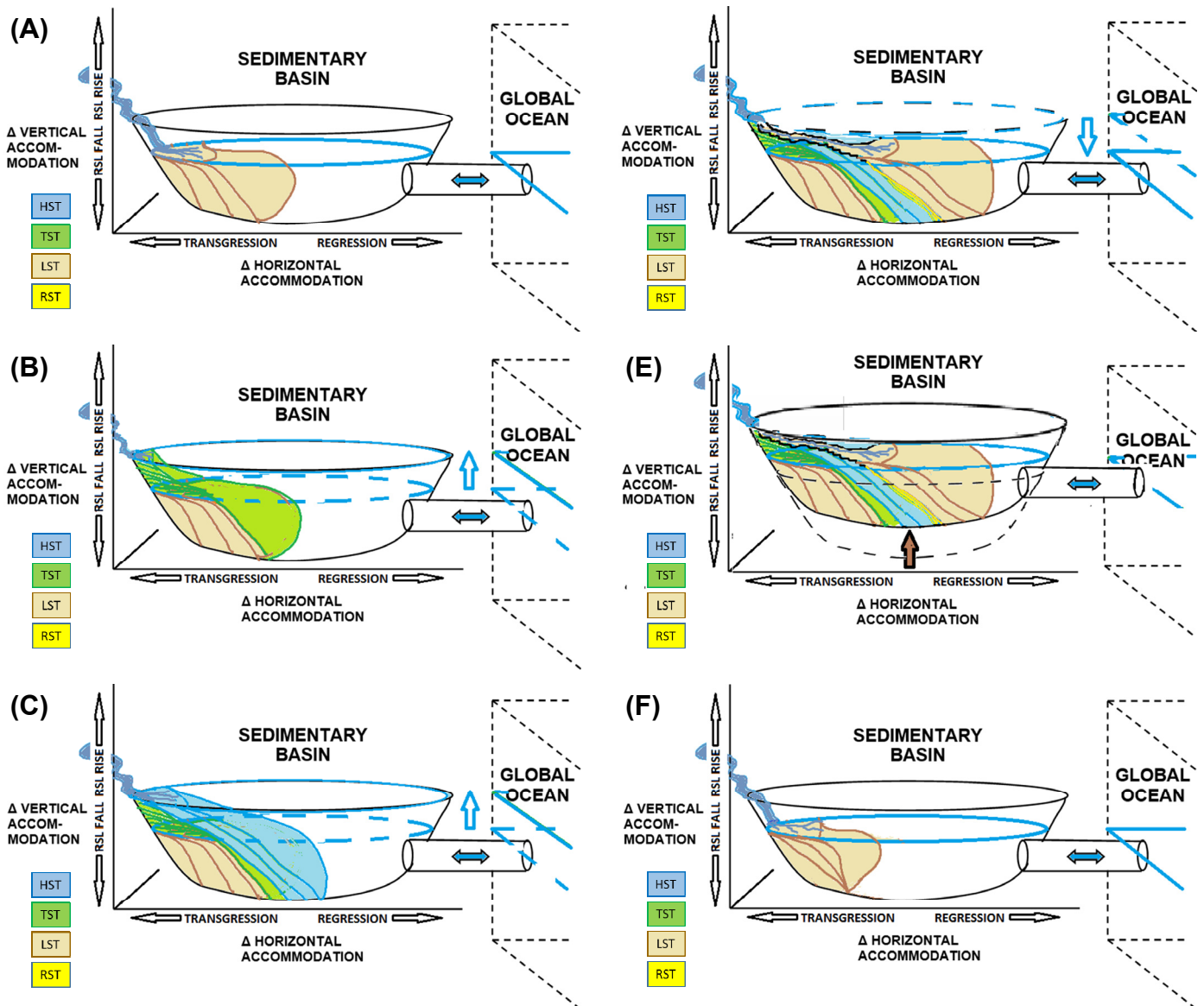


Figure 8. Schematic 3D accommodation models of sedimentary response to varied autocyclic and allocyclic changes in horizontal and vertical space for a basin open to a global ocean. Sedimentary responses are caused by allocyclic and autocyclic changes. See text for parasequence set associations. (A) During an allocyclic stillstand, abundant autocyclic sediment supply provides toplapping progradation, which results in a decrease in the available horizontal space recorded by a regression indicated in brown. (B) Allocyclic global sea level rise with an accompanying increase in both horizontal and vertical space but with weak autocyclic sediment input is recorded by a horizontal onlapping transgression with uplapping and upstepping vertical coastal aggradation indicated in green. (C) Allocyclic global sea level rise accompanies strong fluvial system input relative to marine sediment redistribution processes. Coastal aggradation and progradation indicated in blue fills the available vertical and horizontal space. (D) Allocyclic global sea level fall to global lowstand with strong autocyclic input. Decrease in both horizontal and vertical space is recorded by a dip oriented black unconformity truncating underlying strata with downlapping and downstepping progradation indicated by thin yellow units, which culminate in lowstand regressive deposits indicated in brown. (E) Same accommodation response as (D) but accompanying autocyclic intrabasinal uplift instead of an allocyclic drop in eustatic sea level. (F) With horizontal and vertical accommodation stasis, a stationary shoreline results.

As the cycle continues, the rate of relative sea level rise begins to decrease, indicating the transition to the highstand systems tract stage (HST), illustrated schematically by Figure 8C. If the relative rise in sea level outpaces the sedimentation rate, the decrease in vertical accommodation is revealed by vertical aggradation or stacking of systems which cap this cycle. The prograding sediments develop downlapping patterns onto the underlying MFS during the HST.

Ironically, from a pragmatic standpoint there remains an issue that only through a combination of both seemingly adversarial methods may distinguishing the influences of intrabasinal

autocyclic versus extrabasinal allocyclic processes really be made.

METHODS

There are two principal methods for operationally breaking out a stratigraphic sequence framework: the seismic depositional stratigraphic sequence approach (or "Vail approach") and the genetic stratigraphic sequence approach (or "Galloway approach"). The seismic stratigraphic sequence method developed by Peter Vail and his team at Exxon (Vail et al., 1977) refers to

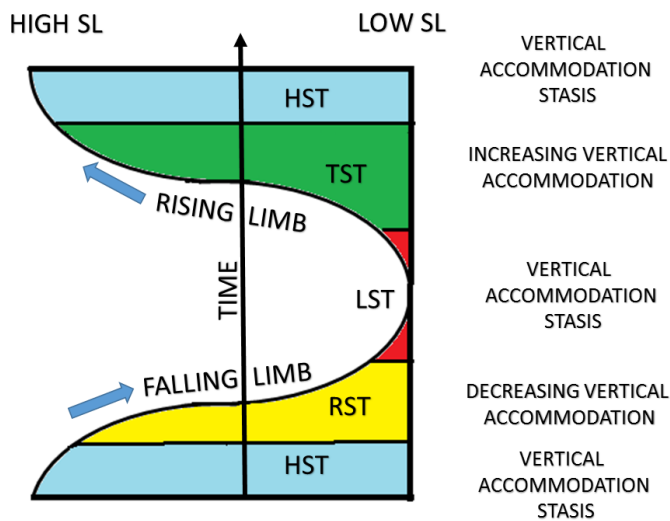


Figure 9. Alloccyclic sea-level curve for one complete sea level cycle with associated vertical accommodation changes. The descending limb of the curve defines the falling stage of sea level and the ascending limb of the curve defines the rising stage of the sea level. Blue indicates HST, Yellow RST, Red LST, and Green TST (modified after Pigott and Abdel-Fattah, 2014).

sequences as a conformable, genetically related succession of strata that are bounded by unconformities or their correlative conformities. This method of sequence delineation is especially facilitated by the interpretation of reflector geometries on regional reflection seismic dip profiles. The genetic stratigraphic sequence method, on the other hand, was developed by William Galloway (Galloway, 1989) and refers to sequences as strata defined by boundaries that record the depositional hiatus that occurs over a transgressed shelf and adjacent slope during maximum marine flooding. The differences in approach are not just semantic. The Vail approach in general more easily images regional unconformities, but suffers in its inability to image flooding surface reflections. By comparison, the Galloway approach, which largely utilizes wireline logs, suffers from less well identifiable intralithological unconformities. However, this depositional approach expounds the importance of the interpretation of low depositional energy deposits (e.g., shales) that progressively overly high energy regressive sediments (e.g., sands), and thus is particularly well suited for less regional work on wireline logs that easily identify shales.

As the Vail approach focuses on identifying sequence bounding unconformities that are regionally pervasive and as reflection seismic tends to resolve at its best third-order cycles, it tends to emphasize the products of alloccyclic processes associated with global eustatic sea level fall. Autocyclic-forced lithologic changes of higher order are generally below conventional seismic reflector resolution and thus can go undetected or even can be potentially miss-interpreted if acoustically tuned. On the other hand, the Galloway approach, focuses on identifying maximum transgressive flooding surfaces in order to define the boundaries between stratigraphic sequences. That is, a fining upward or deepening upward trend in a log motif generally indicates the deposition of low energy deposits above high energy deposits and is interpreted as a transgression. In contrast, a coarsening upward or shoaling upward trend generally indicates the deposition of high energy deposits above low energy deposits, an interpreted regression. As logs tend to emphasize fourth-order cycles, the Galloway method tends to emphasize autocyclic processes. However, the affecting processes are not exclusively autocyclic.

If the flooding surfaces can be shown to be regional (basin-wide) to global in extent, the responsible processes are alloccyclic, indicating a change not in local sea level (such as delta lobe abandonment) but in basin-wide subsidence or global eustatic sea level. Therefore, it is both theoretically and operationally inaccurate to attribute either the Galloway or Vail approach to an exclusive connection to either alloccyclic or autocyclic approaches. While the two techniques can complement each other when both regional seismic and borehole data are combined (e.g. Pigott and Radivojevic, 2010), as this study is field-focused and lacks regional reflection seismic, it emphasizes logs as the major analytical tool, and thus employs the Galloway approach. In the absence then of regional seismic, the global sea level curve augmented by the observed geometry of sand development as a response to interpreted accommodation changes (e.g., Figure 8) will be utilized for assessment of the alloccyclic and autocyclic processes.

To interpret the clastic depositional environments, petrophysical log motifs as pioneered by Fisher (1969) and as have been elaborated upon by Galloway and Hobday (1983) and applied specifically to the Frio by (Holtz and McRae, 1995) were used for the SP log motif interpretation of the wells. Nine distinct depositional environment motifs interpreted from the 113 wells with log data within the study area are schematically shown in Figure 10.

APPLICATION

Accommodation Fill and Facies Interpretation

The autocyclic responses observed in the recorded SP logs are approximately antithetic to the deep resistivity curves, although variations of motif themes are not identical in motif character for all wells. Nonetheless, common patterns predominate. Most representative of these major motifs is the F. L. Blundell 4 well, which is shown in Figure 11. Examination of this well reveals three third-order autocyclic motifs: a Vicksburg-Lower Frio prograding deltaic regression, punctuated by a post Middle Frio transgressive barrier island, then followed by a major Upper Frio prograding deltaic regression.

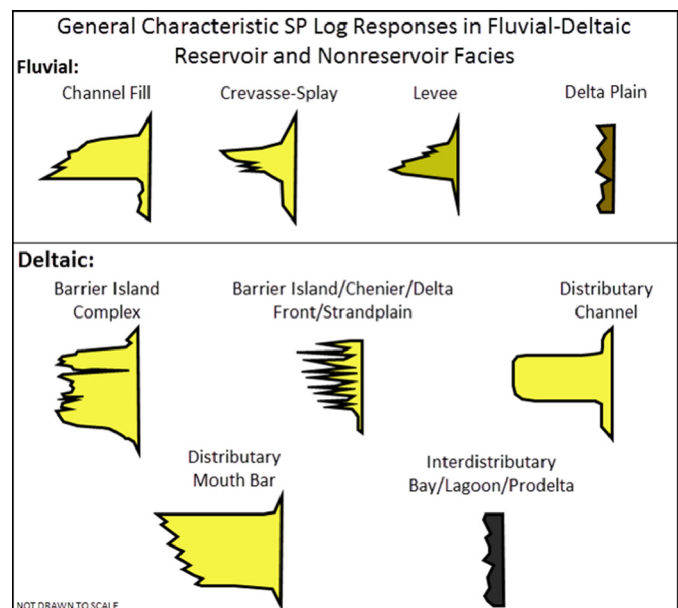


Figure 10. SP log response motifs in Fluvial-Deltaic reservoir and nonreservoir facies environments where the degree of poorer reservoir quality is additionally indicated by darker infill shading (modified after Galloway and Hobday, 1983; Holtz and McRae, 1995).

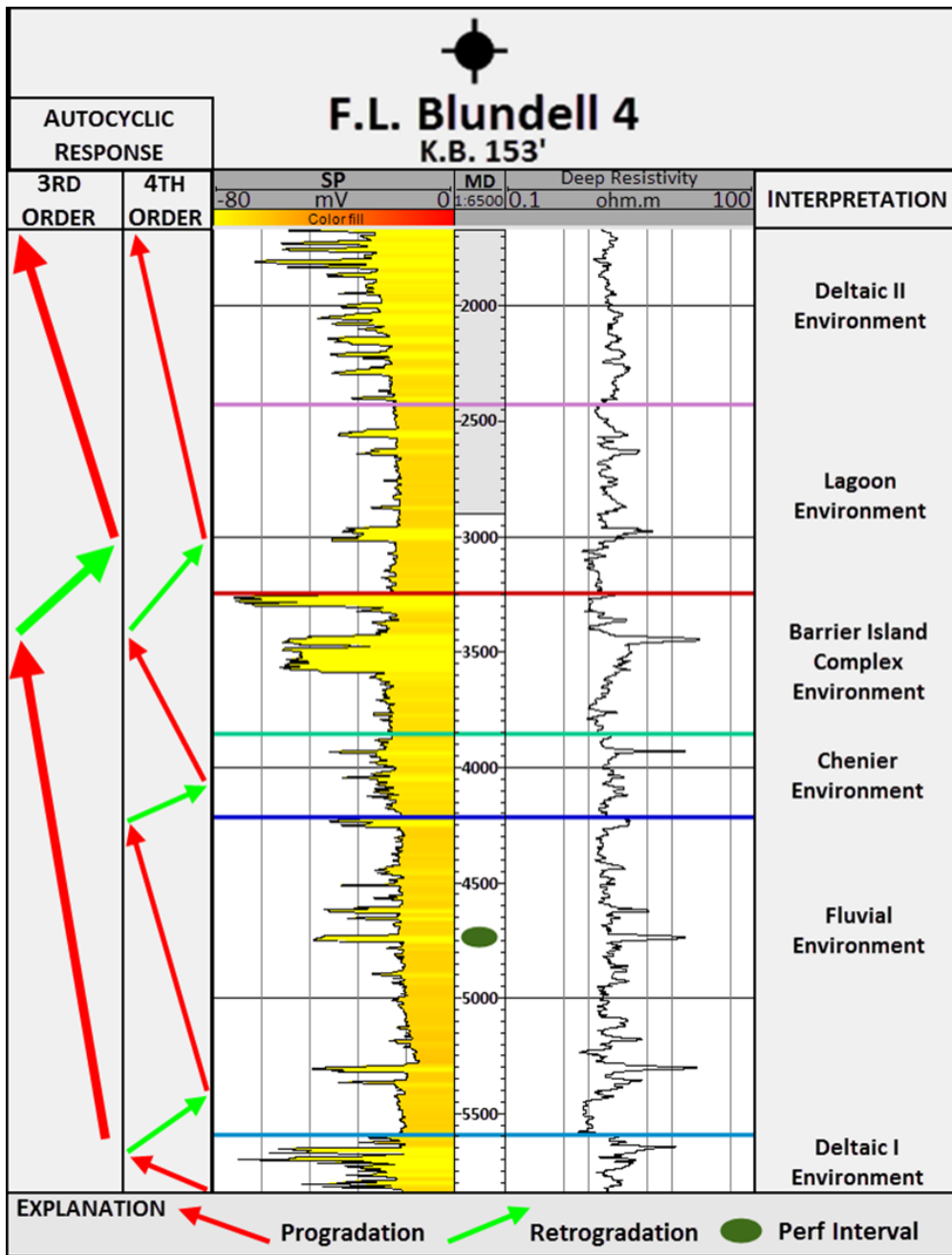


Figure 11. Dominating autocyclic responses observed on for field-representative SP log of the F. L. Blundell 4 well. Three third-order responses identified, and seven fourth-order responses identified. From bottom to top, the colored lines indicate the picked marker bed positions of environment boundaries. Note the three fourth-order transgressive times, which correspond to three fourth-order times of deepening in the global eustatic sea level curve of Figure 2.

Within these third-order cycles are seven fourth-order autocyclic responses that correspond to six identified sand depositional interpreted environments. Commencing in the Late Oligocene, sands of the Vicksburg were deposited and are interpreted to represent the facies of the deltaic I environment during a fourth-order regression. The vertical stacking of sands followed by the preservation of fining upwards motifs at the top of these prograding deltaic sands clearly indicate the increase in both vertical and horizontal accommodation was accompanied by a transgression similar to the model depicted in Figure 8B, thus the delta underlying a flooding marine shale represents an LST. The deposition of the Lower and Middle Frio sands, which are interpreted as facies of the fluvial environment, is punctuated by an ensuing localized fourth-order transgression, followed by another fourth-order regression. A second fourth-order transgression event followed, which led to the initial deposition of the sands of the interpreted crevasse-splay environment, occurring within the Upper Frio; the fourth-order regression and transgressions that

occur within the Upper Frio and Lower Anahuac during the Early Miocene led to the deposition of the sands of the barrier island complex environment, which is marked at the top by the *Heterostegina* Zone, a carbonate-rich sand. This fourth-order transgression that led to the deposition of the sands of the barrier island complex was pencontemporaneous with the beginning of the sand deposition of the lagoon environment. A fourth-order regression during the early deposition of the lagoon environment facies then occurred and continued throughout with the progradation of a second Frio package of sands and silts representing the deltaic II environment. This progradation lead to the diminishment of down-dip horizontal accommodation similar to that described by the model in Figure 8C. The fining upward motif indicates these sands represent an LST to TST transition.

The allocyclic setting for the Late Oligocene to Early Miocene shown in Figure 2 is one of a general falling in global sea level during the Chattian. However, that there exists the preservation of a Frio clastic wedge sedimentary record for this period

ACCOMMODATION DIAMOND

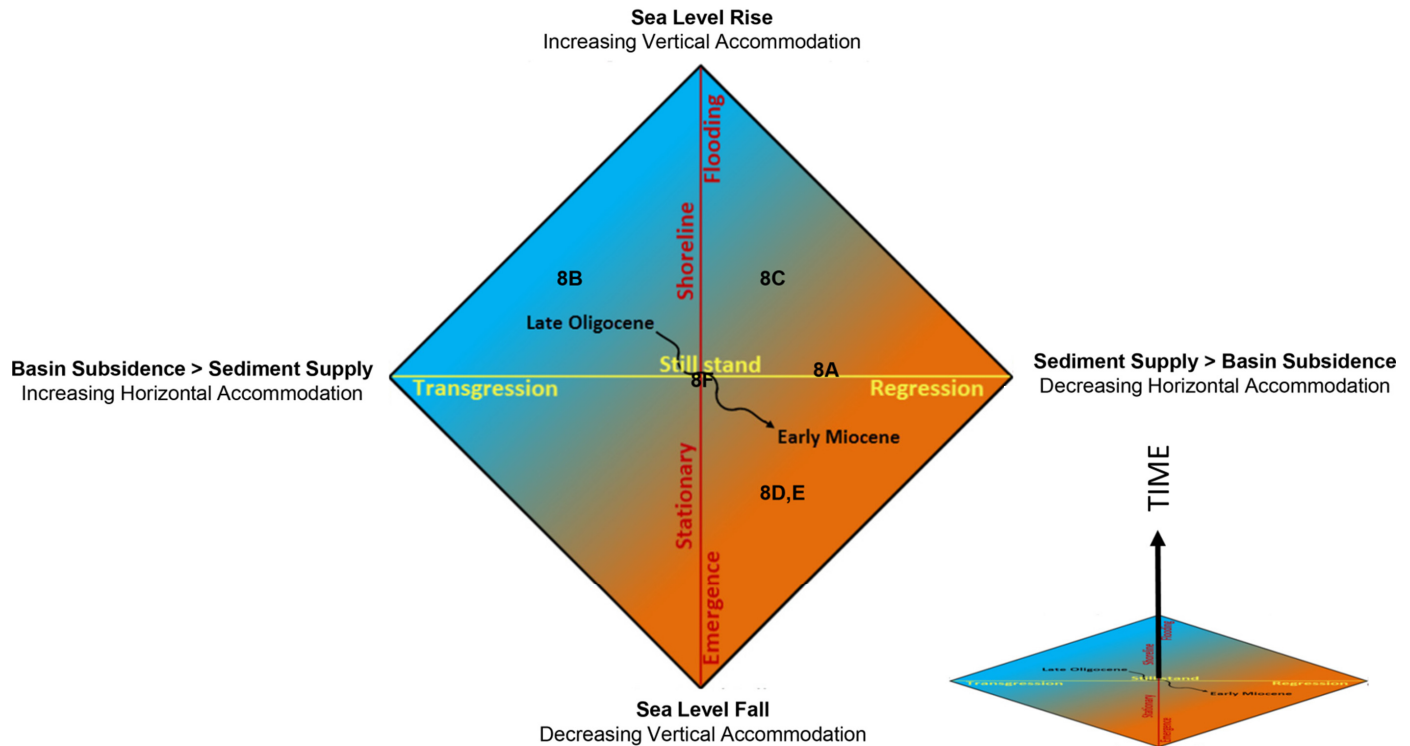


Figure 12. Quaternary accommodation diagram, which portrays the sedimentologic response to the principal allocyclic and autocyclic drivers affecting changes in accommodation. Numbers 8A–8F refer to relative positions of the accommodation models of Figure 8. The curved black line schematically represents the Frio depositional facies in Jim Wells and Nueces counties of South Texas as an evolutionary and cumulative response to both autocyclic and allocyclic processes. The time axis is orthogonal to the plane of accommodation drivers.

is evidence that deposition of the Frio was less influenced by a global eustatic sea level fall and more by autocyclic basin subsidence as the basin margin foundered and relative sea level rose. The resulting sedimentary geometry indicates decreasing horizontal accommodation updip, but increasing accommodation downdip. However, when the three fourth-order allocyclic eustatic rises occurred that accompanied continued basin subsidence, the sediment input was no longer sufficient to provide regression and three corresponding transgressions occurred (compare Figure 11 to global sea level curve of Figure 2). Thus the interpreted motifs of Figure 11 reveal the pulses of regressional facies that are disjunctive to the allocyclic signal of a falling global sea level and illustrate that autocyclic processes were the main driver. Confirming this overall decrease in horizontal accommodation owing to autocyclic processes that additionally caused local basin subsidence are estimates of sediment deposition related to the progradation of this continental platform that exceed 15,000 vertical ft of sediment and laterally extend up to 50 mi in width (Galloway et al., 1982). This massive sediment deposition within the basin allowed for sediment infill accumulations to eventually prograde gulfward beyond the underlying Mesozoic shelf margin and onto transitional oceanic crust. Thus, Frio deposition was volumetrically primarily the result of autocyclic processes, not allocyclic processes. Yet, allocyclic events are still recorded as the three fourth-order cycles of sea level rise corresponding to the three fourth-order observed transgressive systems tract motifs (compare Figures 2 and 11). It is useful to portray the evolutionary interplay between the interpreted autocyclic and allocyclic drivers. Summarizing this relationship, the accommodation diamond of Figure 12 schematically illustrates the combined influence of the allocyclic and autocyclic drivers deemed responsible for the observed sedimentary facies and as-

sociated interpreted environments of these Frio depositional systems. The 3D accommodation diagrams of Figure 8 are additionally positioned for reference.

Field Reservoir Facies Geometries

To determine relationships between facies and sand geometries and to help further elucidate allocyclic and autocyclic processes, it is informative to examine maps of these six defined Frio clastic environments with respect to net sand thickness. Beginning at the base, Figure 13A is a net sand map of the deltaic I environment, which was deposited as a lower Chattian Vicksburg sand in the early Norias delta system (Galloway et al., 1982). These sands laterally exhibit three distinct delta lobes within the study area as is indicated by regions of high net sand accumulation. The interpreted deltaic I environment has a mean net sand of 364 ft, with a maximum of 578 ft and a minimum of 251 ft.

The net sand map of the interpreted fluvial environment shown in Figure 13B, which represents part of the Gueydan Fluvial System of Galloway et al., (1982) was deposited as a mid Chattian sand of the Lower and Middle Frio. The map reveals the fluvial sands to have been deposited within a topographic low of the deltaic I environment. The occupation of these distributary channels in this low together with their observed abrupt bases (Fig. 11) suggests downcutting during a decrease in vertical accommodation accompanying a relative sea level fall. Those channels with abrupt tops indicate upper RST coastal plain terraces while those with fining upward tops indicate lower RST to LST fluvial sands capped by transgressive shales (comparable with schematic Figures 8E and 8B, respectively). The capping transgressive TST shale (of a flooding lagoonal environment),

provides an excellent top seal for these reservoir sands. The interpreted fluvial environment has a mean net sand of 368 ft, with a maximum net sand of 862 ft and a minimum net sand of 108 ft.

Figure 13C is the net sand map of the interpreted crevasse-splay environment, which was deposited as the Upper Frio during the latest Chattian. These sands show similar depositional characteristics to that of the fluvial environment with respect to regions of high and low net sand deposits and thus indicate environmental associations with those fluvial sands. The interpreted crevasse-splay environment has a mean net sand of 143 ft, with a maximum net sand of 443 ft and a minimum net sand of 36 ft.

The sands representing the interpreted barrier island complex environment displayed in Figure 13D, and named the Greta barrier island system by Duncan (1983) were deposited during the earliest Aquitanian as the Anahuac Formation. This map reveals the major sand lineation of this north-trending barrier island system. Within these fields, the Greta barrier island complex environment is represented by a mean net sand of 291 ft, with a maximum net sand of 489 ft and a minimum net sand of 156 ft.

Figure 13E illustrates the net sand map of the interpreted lagoon environment. These mid-Aquitania sands of the Anahuac Formation trend parallel to the Greta barrier island complex environment and are interpreted to represent intralagoonal storm washover deposits from the barrier island. The lagoon environment has a mean net sand of 295 ft, with a maximum net sand of 612 ft and a minimum net sand of 89 ft.

The net sand map of the interpreted deltaic II environment shown in Figure 13F represents the upper lobe of a later Aquitanian Norias delta system. These sand deposits of the prograding Anahuac Formation reveal three individual deltaic lobes indicated by the regions of high net sands. The mean net sand of the deltaic II environment is 801 ft, with a maximum net sand of 1402 ft and a minimum net sand of 376 ft.

The two cross sections in Figure 14 illustrate the relationship between subsurface formations and depositional environments within the study area. The datum is the *Heterostegina* Zone, which transgresses the barrier island complex during a time of diminished clastic input and implies increasing horizontal and vertical accommodation analogous to the model shown in Figure 8B. Figure 14A illustrates cross section A–A' which runs perpendicular to the axis of Frio deposition and throughout the majority of the Captain Lucey Field. Figure 14B illustrates a depositional dip-oriented cross section F–F' that runs parallel to the axis of Frio deposition and extends from the Captain Lucey Field into the Richard King Field.

As reviewed previously in the Field Production History section, both the Captain Lucey and Richard King fields are affected by the post-depositional structuring along of the Frio Fault Zone. Figure 15 demonstrates the effects of such structuring adjacent to the faults for the Lower Frio. Observe that for both fields major production occurs on structural highs proximal to the faults suggesting for these shale-encapsulated sands the fault zones are zones of diminished permeability and thus likely with high shale gouge ratios.

To summarize these environmental interpretations, Figure 16 illustrates schematically a map view of these major Oligocene-Miocene South Texas Frio depositional systems during one fourth-order rising limb in the eustatic sea level curve. The autocyclic depositional systems are adjusting to increased vertical and horizontal accommodation. We shall now attempt to characterize the producing reservoirs of these representative sand facies.

DECLINE CURVE ANALYSIS

Theory

Production decline curve analysis (PDCA) for producing oil and gas fields is a classic method for examining well perfor-

mance, forecasting future production, and determining value of the producing asset. The theory of decline curve analysis is based on the analysis of J. J. Arps (1945) that showed most reservoir depletion follows a hyperbolic shaped decline curve. According to Arps, the three most common forms of the general hyperbolic decline equation include exponential ($b = 0$), hyperbolic ($0 < b < 1$), and harmonic ($b = 1$), as is shown schematically in Figure 17.

Production decline curve analysis involves the delineation of a production decline trend line with the best fit to the data. The trend line then is assumed to be representative of the overall decline in hydrocarbon production over time and thus may be used to forecast future hydrocarbon production and its interpreted decline for a given well. The exponential decline is regarded as the most simple and conservative decline rate, describes fluid expansion, and serves as an approximation of estimated ultimate recovery (EUR) where the decline rate is constant versus time. The hyperbolic decline is expressed as a non-linear curve fit that is used to generate b -values (hyperbolic decline exponents). Where the decline rate is not constant, the hyperbolic decline describes solution gas drive and provides an EUR between that of a hyperbolic and a harmonic decline rate. The harmonic decline expresses the decline rate as directly proportional to flow rate, describes efficient water drive where rate versus time appears as a straight line on a semi-log plot. Of the three equations, the harmonic decline approximation provides the most optimistic approximation of EUR (Foster, 2012).

For this field study, the decline curve analysis incorporates both exponential and hyperbolic decline curves for the selected wells. The following variables described in detail by Poston and Poe (2008) and Foster (2012) were determined:

b = hyperbolic decline exponent,

D_i = initial continuous decline rate, and

q_i = initial production rate (start of production).

Cumulative production (Q_p) is calculated through the general hyperbolic decline rate equation:

$$Q_p = \frac{q_i}{(1-b)D_i} \left[1 - (1 + bD_i t)^{-1/b} \right] \quad (1)$$

where t is the cumulative time since start of production in years. The current production rate (q) at a given time was determined according to the method advanced by Fetkovich et al. (1996):

$$q = \frac{q_i}{(1 + bD_i t)^{1/b}} \quad (2)$$

Once the above variables have been determined, the rate-match point (q_{Dd}) and the time-match point (t_{Dd}) may be solved using the following equations:

$$q_i = \left(\frac{q}{q_{Dd}} \right)_{MP} \quad (3)$$

$$D_i = \left(\frac{t_{Dd}}{t} \right)_{MP} \quad (4)$$

The rate-match point (q_{Dd}) and the time-match point (t_{Dd}) may then be used to solve for the transient flow best fit dimensionless radius (R_{eD}) through either of the following equations (Foster, 2012):

$$q_{Dd} = \left(\ln(R_{eD}) - \frac{1}{2} \right) q_D \quad (5)$$

Net Sand Map: Deltaic I Environment

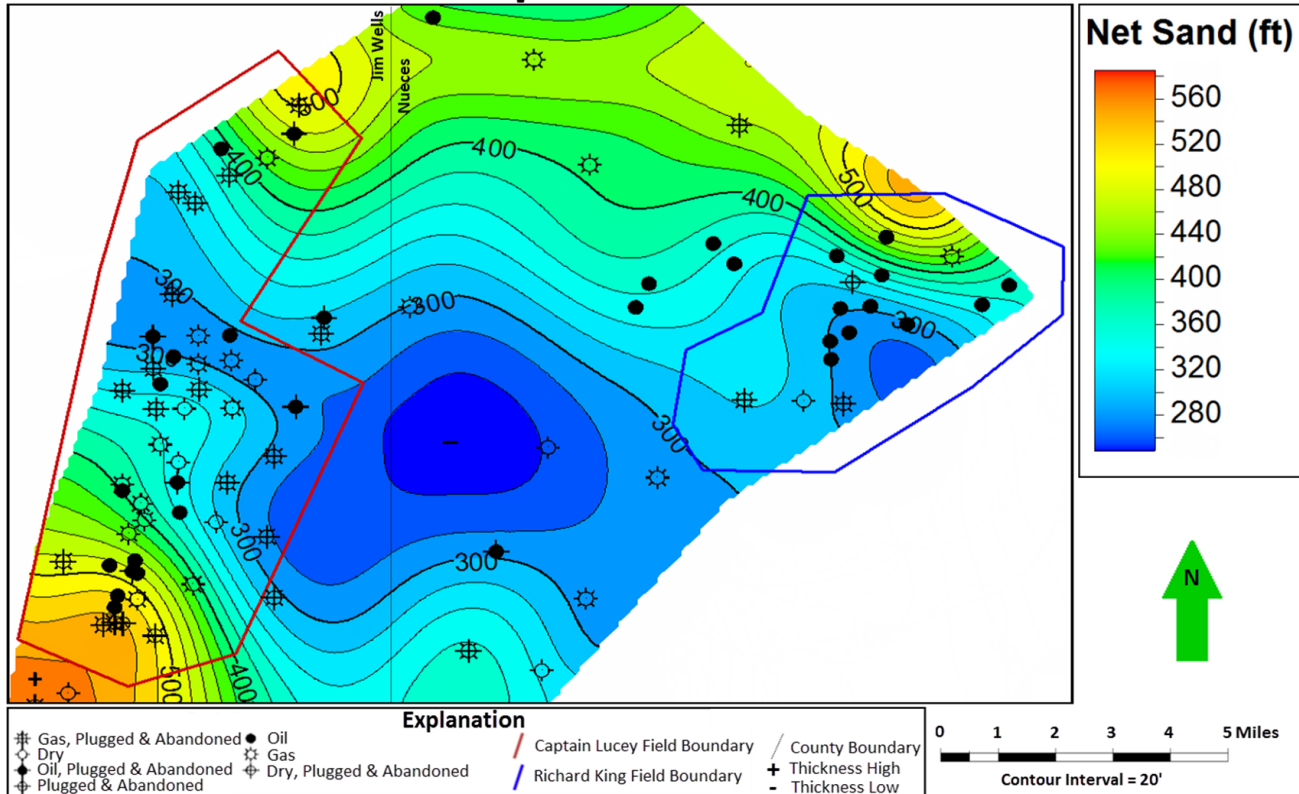


Figure 13A. Net sand map of the interpreted deltaic I environment, which represents Vicksburg sands of the Late Oligocene (Chattian).

Net Sand Map: Fluvial Environment

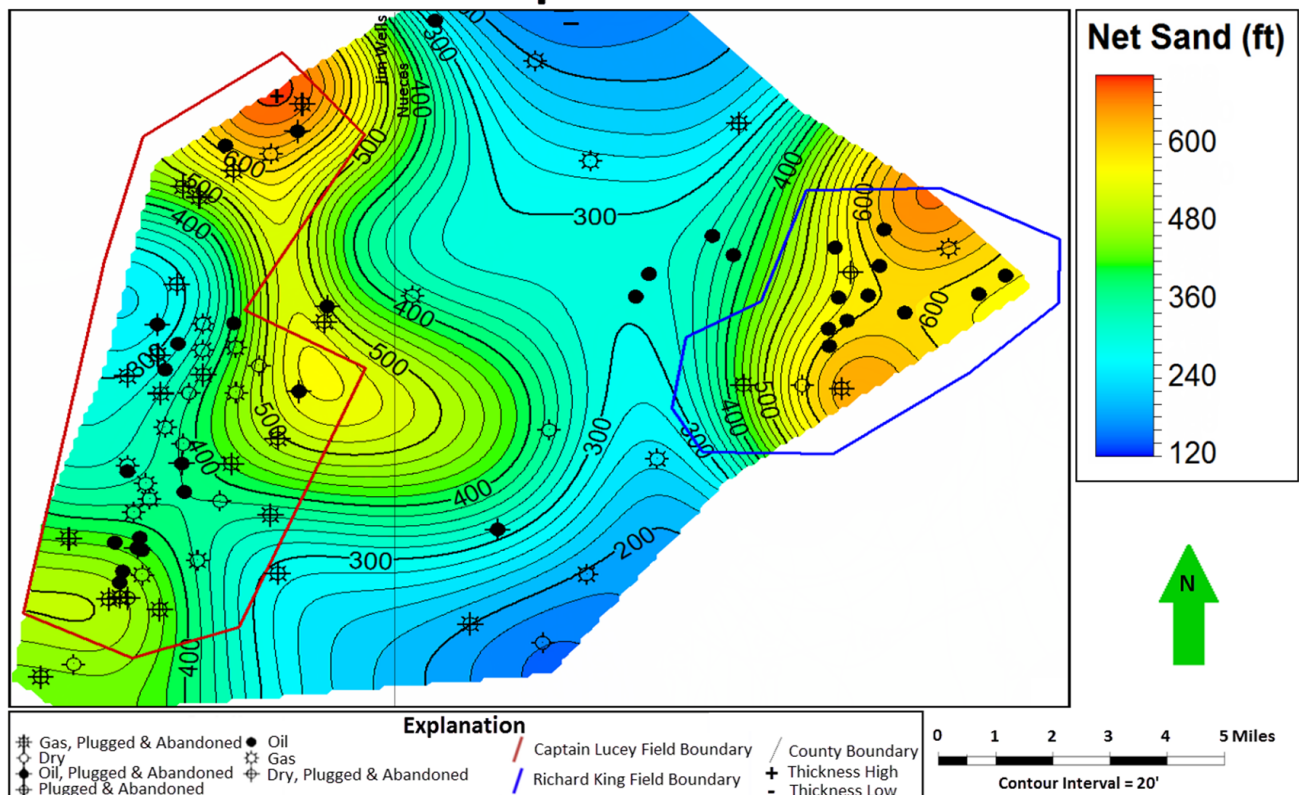


Figure 13B. Net sand map of the interpreted Gueydan fluvial environment, which represents the Lower and Middle Frio of the Late Oligocene (Chattian).

Net Sand Map: Crevasse-Splay Environment

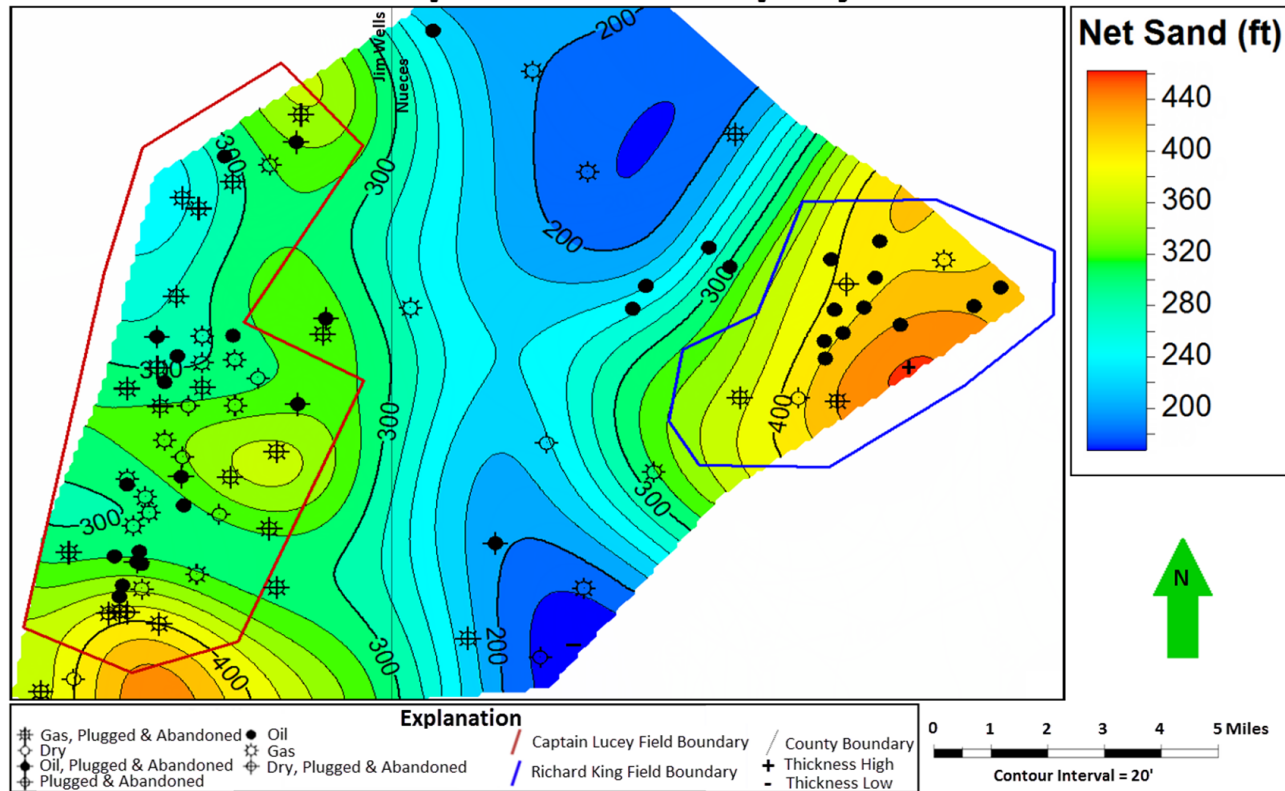


Figure 13C. Net sand map of the interpreted crevasse-splay environment, which represents Upper Frio sediments deposited during the Late Oligocene (Chattian).

Net Sand Map: Barrier Island Complex Environment

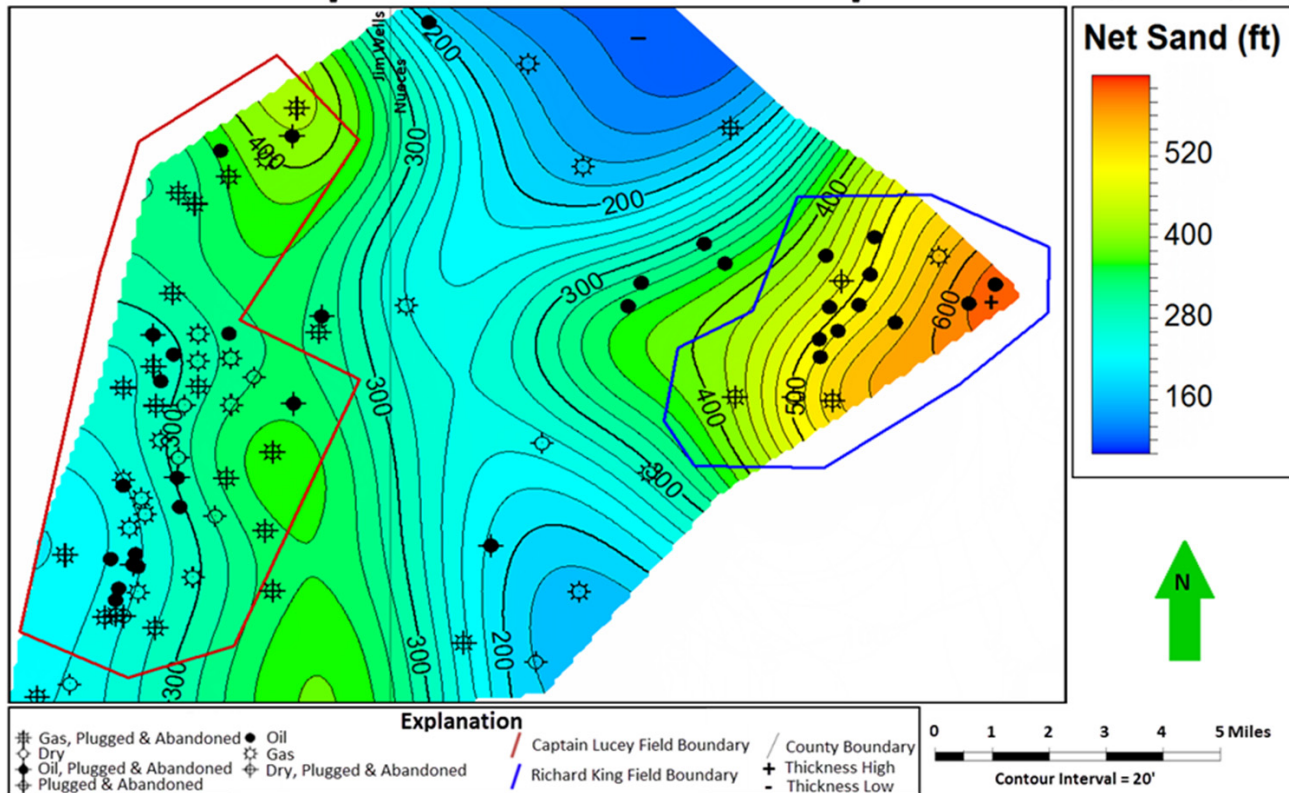


Figure 13D. Net sand map of the interpreted barrier island complex environment, which represents the Anahuac deposits of the Early Miocene (Aquitanian).

Net Sand Map: Lagoon Environment

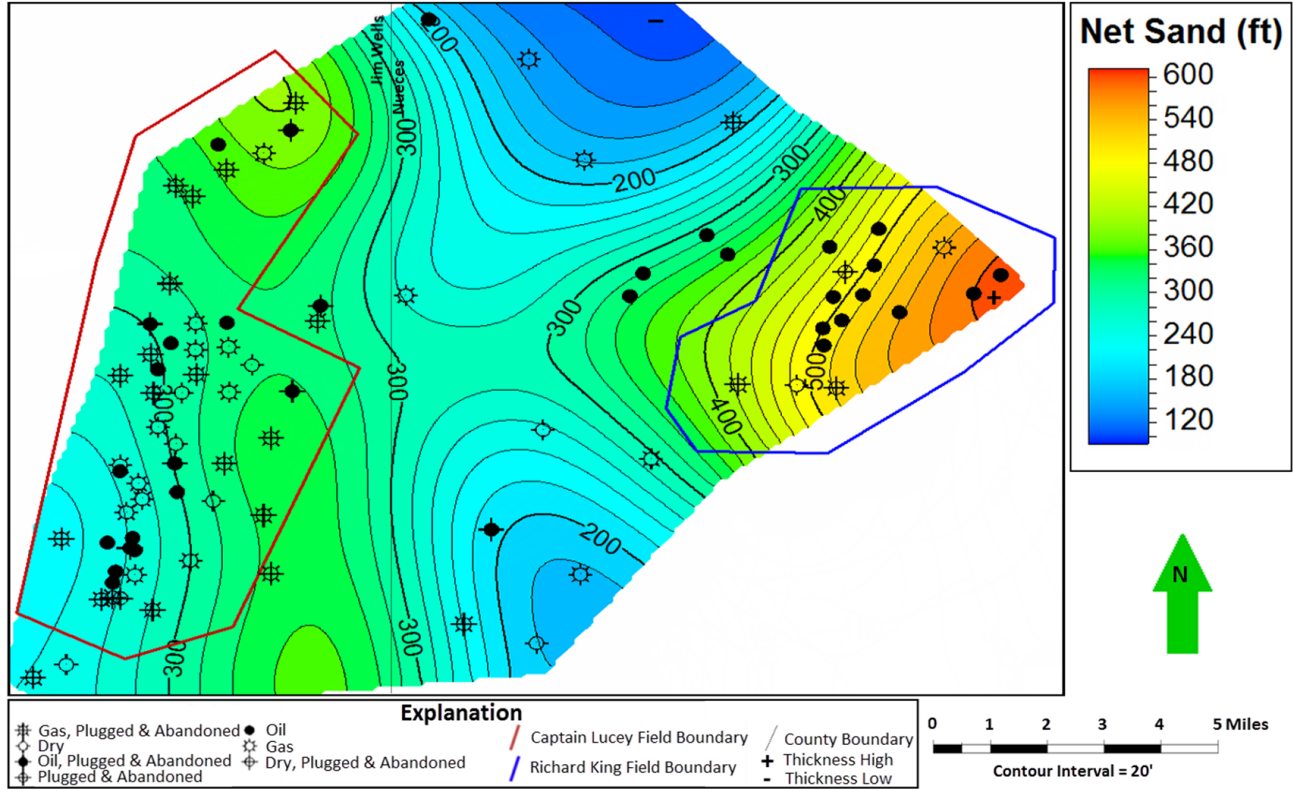


Figure 13E. Net sand map of the interpreted lagoon environment, which represents Anahuac deposits of the Early Miocene (Aquitanian).

Net Sand Map: Deltaic II Environment

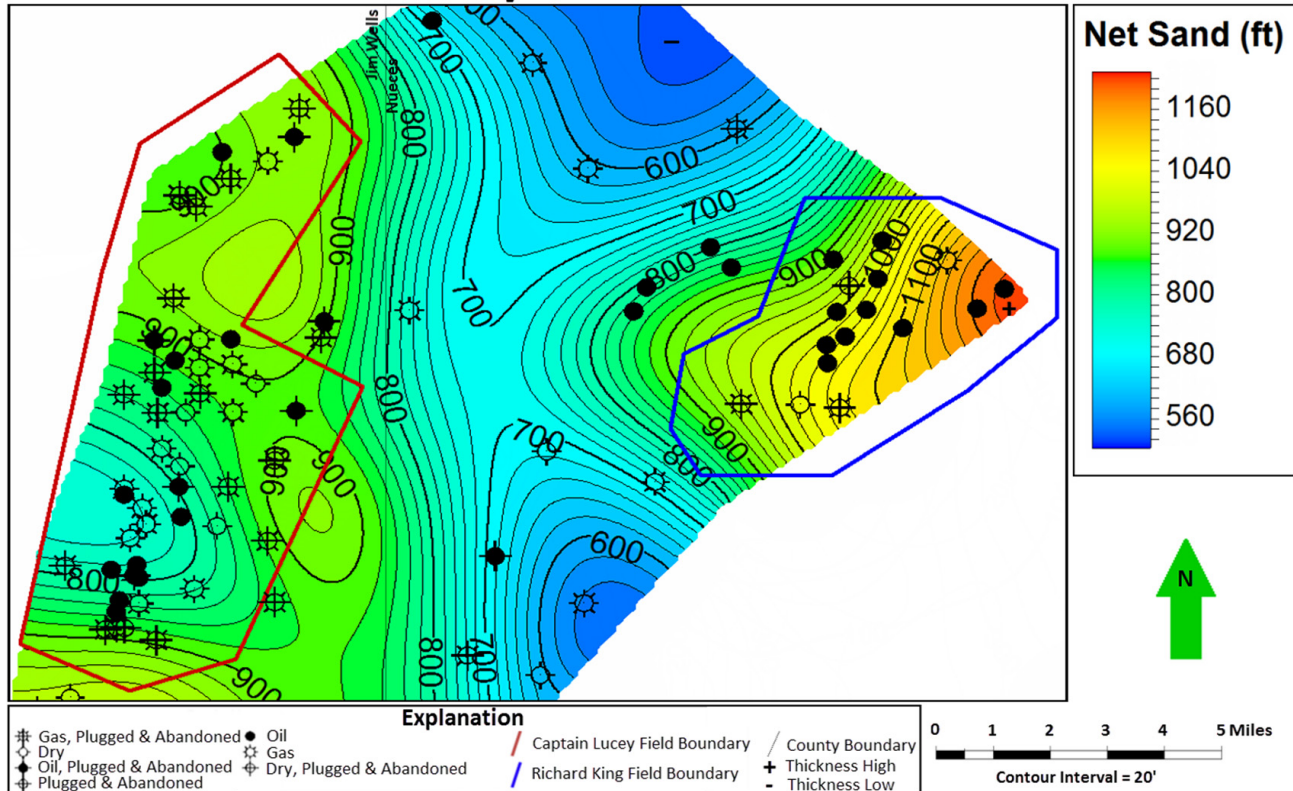


Figure 13F. Net sand map of the interpreted deltaic II environment, which represents Anahuac deposits of the Early Miocene (Aquitanian).

$$t_{Dd} = \frac{t_D}{\frac{1}{2}(R_{eD}^2 - 1)(\ln(R_{eD}) - \frac{1}{2})} \quad (6)$$

where t_D is the time rate (for transient flow period).

Two particular variables that can be derived from PDCA and that can augment the preceding variables for geological characterization and interpretation are drainage area (DA) and permeability (k). These two variables were derived by Fetkovich et al. (1996) and form the principal method employed here.

Method

For the hydrocarbon producing facies positioned within the previously interpreted sequence stratigraphic intervals, following the geometric character, the second and third reservoir components were determined: the calculated theoretical permeability (k) and drainage area (DA). Three procedural steps were involved.

The first step was to review historical production trends for wells owned and operated by Quatro. The goal of this step was to identify wells that possessed historical hydrocarbon production trends for known producing reservoirs that accurately portrayed that specific depositional environment's production characteristics. It was important to not incorporate historical hydrocarbon production trends for wells that incurred mechanical failures (e.g., poor cement jobs, pump problems, casing leaks, etc.) or for wells that exhibited excessive hydrocarbon production declines owing to abnormal reservoir pressure depletion. The company data provided both documentation of these mechanical failures as well as the perforation intervals for measured depths within a given well, which allowed for the association of hydrocarbon production to depositional environments. Cumulative oil and gas production for all Quatro wells in the Captain Lucey and Richard King fields was tabulated. Following the removal of problematic wells, of the currently active 20 wells, 18 reservoirs from 12 wells of these two fields ultimately were identified as candidates for production decline curve analysis.

For the second step, production decline curve analysis for these eighteen reservoirs was then performed by using PHDWin Integrated Economics and Decline Curve Analysis software (herein simply termed PHDWin PDCA). PHDWin PDCA software solved the necessary variables described in the preceding equations. These variables were then applied to the following Fetkovich decline curve equations (Fetkovich et al., 1996) in order to characterize the reservoir permeability (k_{DCA}) and drainage area (DA_{DCA} [ac]).

Using the Fetkovich type curve match approach, k_{DCA} can be solved for from the rate match point equation:

$$k_{DCA} = (\ln(R_{eD}) - \frac{1}{2}) \left(\frac{141.2\mu b}{h(p_i - p_{wf})} \right) \left(\frac{q}{q_{Dd}} \right) \quad (7)$$

where μ is the viscosity ($\mu_{gas} = 0.0213$ cp; $\mu_{oil} = 1.84$ cp), h is the height of the reservoir (perforation interval) (ft), p_i is the initial pressure (psi), and p_{wf} is the shut-in pressure (psi). The drainage area may then be calculated from rate and time match points:

$$DA_{DCA} = \frac{5.615b}{\Phi_{density} h c_t (p_i - p_{wf})} \left(\frac{t}{t_{Dd}} \right) \left(\frac{q}{q_{Dd}} \right) \quad (8)$$

Where $\Phi_{density}$ is the average density-derived porosity for a potential reservoir, and c_t is the compressibility ($c_{t\ gas} = 0.000154$; $c_{t\ oil} = 0.000015$).

The third and final step of this reservoir characterization analysis involved the delineation of the hydrocarbon producing

depositional environments and their associated interpreted sequence stratigraphic intervals. This step helped to define average values for the hyperbolic decline exponent (b), initial continuous decline rate (D_i), initial production rate (start of production) (q_i), along with permeability (k_{DCA}), and drainage area (DA_{DCA}) for a given oil or gas reservoir and its associated depositional environment and sequence stratigraphic interval. These data parameters were necessary in order to determine the producing volumetric analysis of the field study area.

Application

PDCA was performed on 18 separate reservoirs within these 12 selected wells of these two fields located within the study area (Fig. 18). The identification of the depositional environments was based on the interpreted SP log motifs. The interpreted best fit curves superimposed on these type production decline curves are the most representative of the actual quantitatively derived decline curve parameters for the individual wells. Representative production decline curves for oil and gas reservoirs of the depositional environments identified in the study are found in Figures 19A through 19E.

Calculated permeability (k) and drainage area (DA) values for the identified oil and gas reservoirs by depositional environment are summarized in Table 1. The PDCA parameters reveal that delta front and distributary mouth bar oil-bearing reservoirs possess the greatest drainage areas (DA) and permeabilities (k), followed by oil-bearing fluvial channel reservoirs. The decline curve analysis reveals that barrier island gas-bearing reservoirs maintain the greatest drainage area (DA) and permeability (k), followed by fluvial channel, and, finally, crevasse-splay reservoirs. Log-derived porosities for these sand reservoirs do not vary greatly but are highest in the barrier island (25%) and are lowest in the crevasse splay environments (20%).

SYNTHESIS

Petrophysical log motifs of 113 wells in the adjoining Captain Lucey and Richard King fields of Jim Wells and Nueces counties (Fig. 1) correlated and constrained with biostratigraphy and the global sea level curve reveal the greater overprint of fourth-order autocyclic processes of regression and transgression upon a general third-order Chattian allocyclic sea level fall. Five reservoir sand environments sealed by TST marine shale in this part of the Frio wedge are: LST delta 1, RST–LST delta plain distributaries, distributary crevasse splay, TST barrier island complex, and LST–TST delta 2. The Oligocene-Miocene Frio in these two fields reveal a subsiding shelf of fourth-order autocyclic processes of regression and transgression within a general third-order allocyclic sea level fall.

Fetkovich PDCA of 18 reservoirs from 12 of 20 currently active wells producing oil and gas from these two fields shows a systematic relationship between calculation-extracted reservoir elements and their associated depositional environments (Table 1). The interpreted LST–TST deltaic I and LST–TST deltaic II environments (principally delta front sands) exhibit the best reservoir quality of the five, exhibiting the lowest linear decline rates, highest average flow permeabilities (80 md) and largest drainage areas (290 ac) perhaps owing to sand amalgamation during the transition from LST to TST. A close second in drainage area is the transgressive barrier island sand, which responded to increased horizontal accommodation as the shelf subsided accompanied by diminished sediment input (river avulsion and delta switching?) with large drainage area (251 ac) but lower average flow permeability (7 md). Likely the poorer reservoir permeability of these sands was caused by the diminishment of textural maturity owing to their interspersed within lagoonal muds. The RST–LST fluvial sand exhibits the fastest decline rates but with large drainage area (214 ac) possibly owing to the

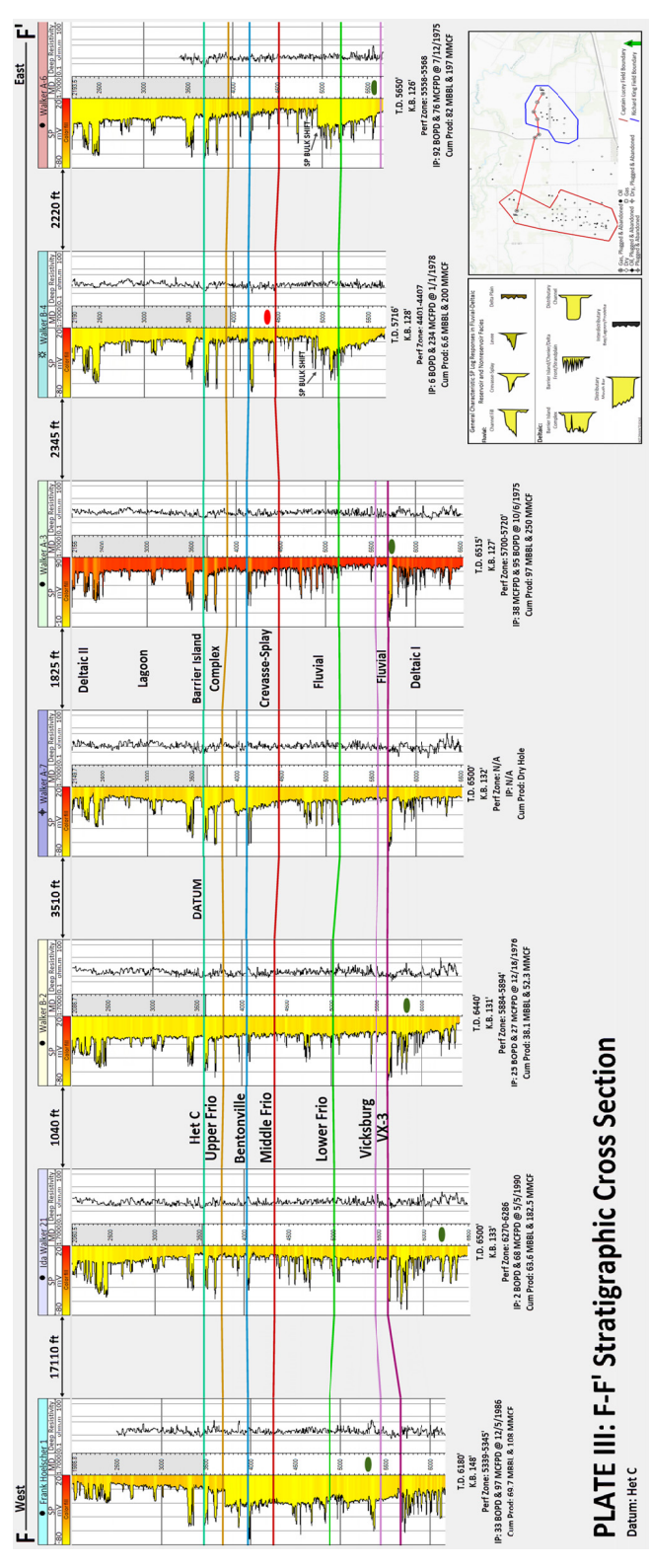
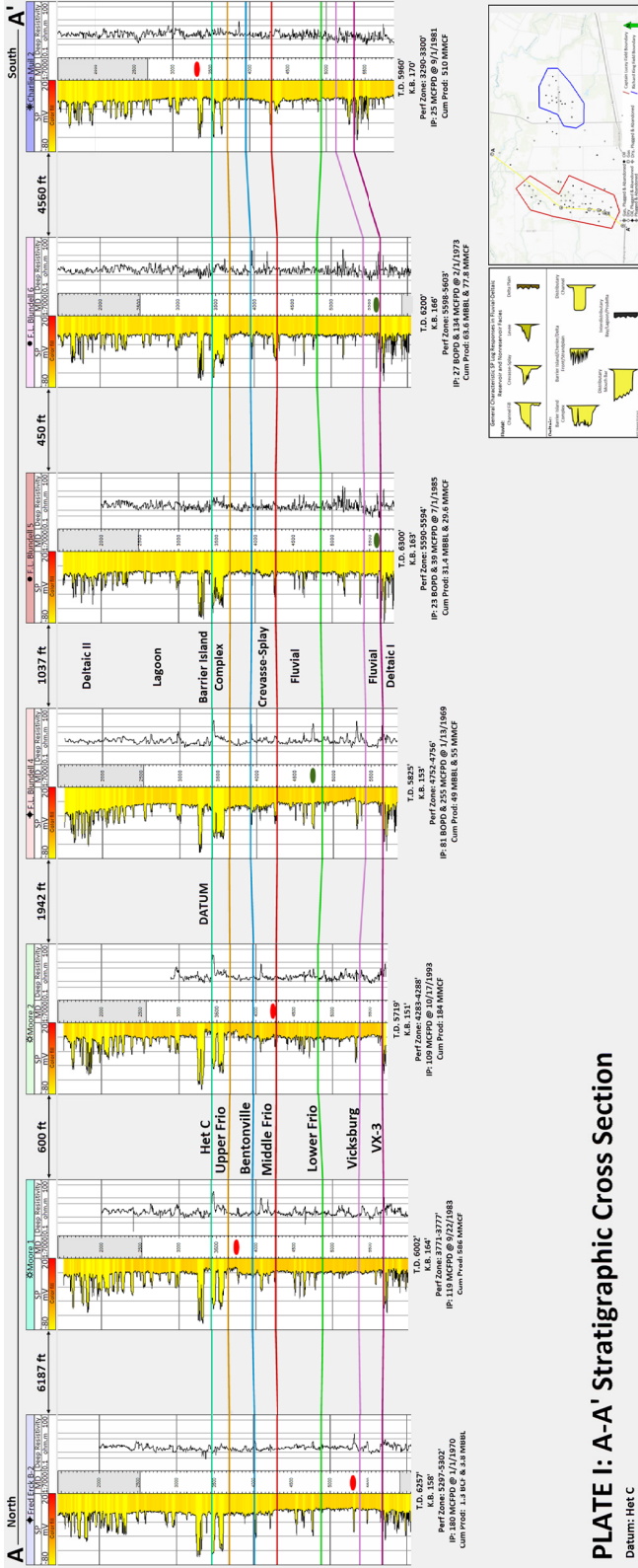


Figure 14. Stratigraphically correlated cross sections through the study area. Shaded colors indicate shaliness with yellow indicating high sand and red high shale. (A, top) Depositional strike cross section A-A'. (B, bottom) Depositional dip cross section F-F'.

Structure Map: Lower Frio

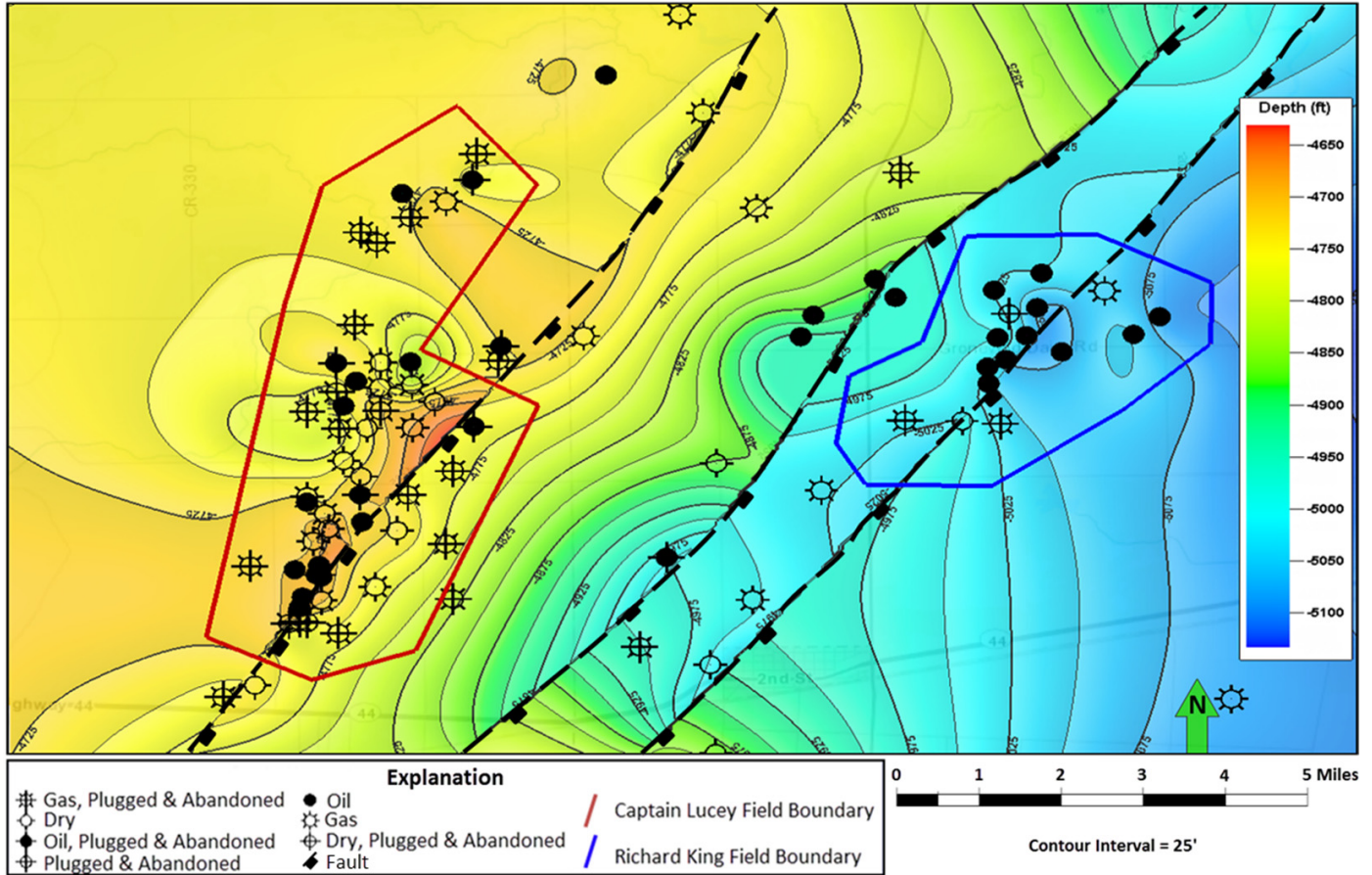


Figure 15. Structure map of Lower Frio illustrating three faults within the Frio Fault Zone and the predominance of oil and gas wells on structural highs adjacent to the faults.

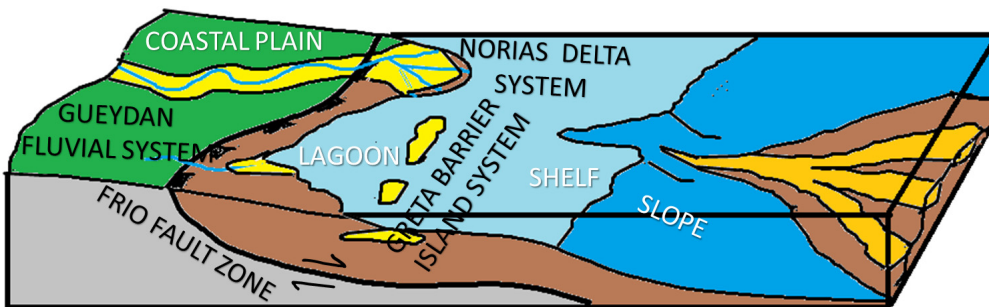


Figure 16. Schematic representation of Oligocene-Miocene environments of major South Texas Frio depositional systems of the study area region during one fourth-order rising limb in the eustatic sea level curve. The autocyclic depositional systems are adjusting to increased vertical and horizontal accommodation space.

extent of its incised valley boundaries and modest average permeability (32 md). The poorest reservoir quality is the rapidly declining production of the crevasse splay sand with lowest permeability (1 md) and smallest drainage area (110 ac).

These relationships associated with the comparison of decline curve analysis to depositional environment characterization of these RST, LST, and TST and fault sealed reservoirs can assist in pre-delineation drilling reservoir characterization and potentially allow for preliminary evaluations of bypassed, behind-pipe pay. For example, while the sands encountered in one borehole (e.g., untested sands in Figure 5) may indicate such non-commercial reservoir characteristics as thin geometries, poor porosities and permeabilities owing to immature sediment tex-

tures or diagenetic cementation, low oil gravity, and/or high water cut, the PDCA of these sands in adjacent wells may point to these effects as being localized owing to distal facies effects, syndepositional or postdepositional structuring affecting updip oil biodegradation, updip calcite supersaturated waters, etc. Therefore, while wireline and core analysis allow the determination of thicknesses and permeabilities within the wells vertically, the areal extent of a draining reservoir cannot be quantified without the lateral dimension. It is the lateral dimension with all its irregularities, heterogeneities, and compartments that the PDCA commences to answer. Moreover, the results of this study strongly suggest that a relationship between decline curve analysis and depositional environments exists and indicate the poten-

Curve Types for Decline Curve Analysis

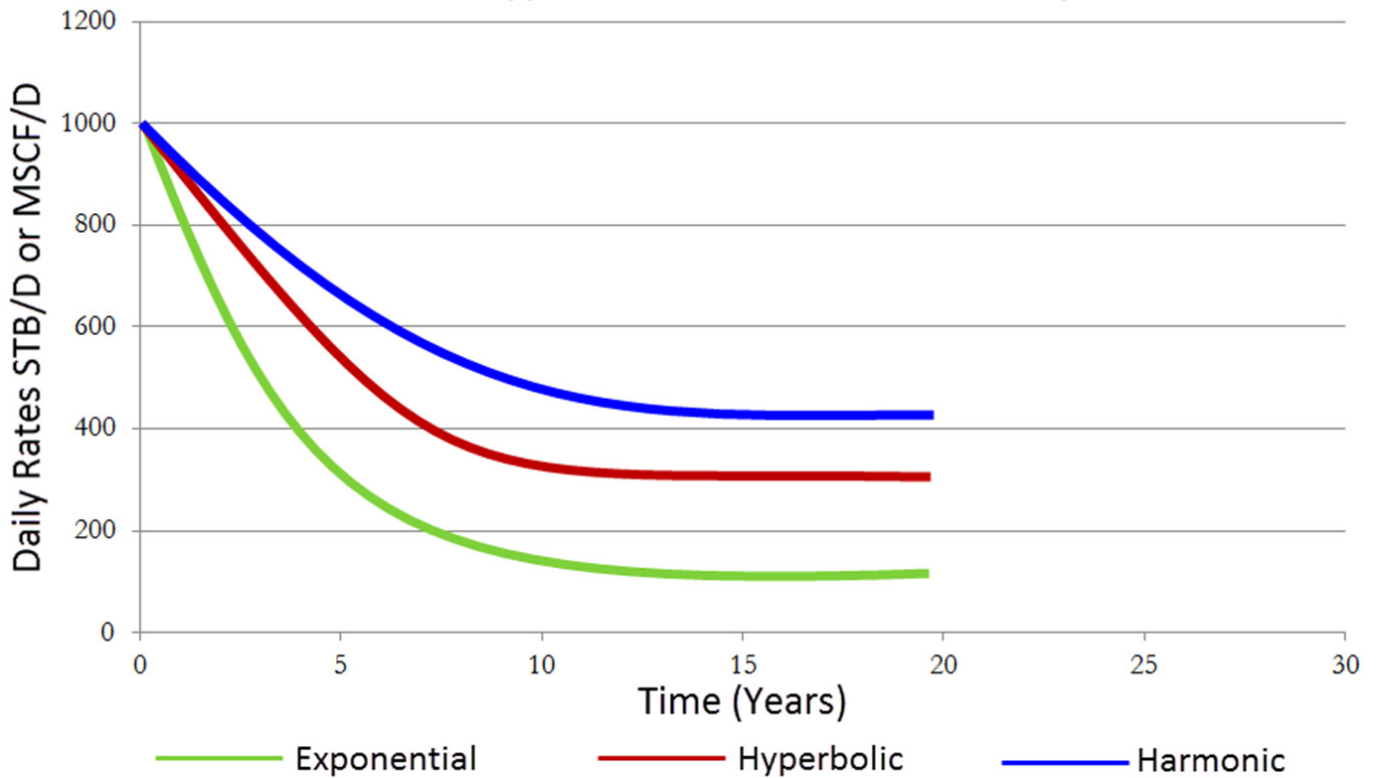


Figure 17. Graphic examples of the three most common forms of decline curve expressions within the general hyperbolic decline equation. The curves are exponential ($b = 0$) which describes fluid expansion, hyperbolic ($0 < b < 1$), which describes solution gas drive, and harmonic ($b = 1$), which describes efficient water drive (modified after Foster, 2012).

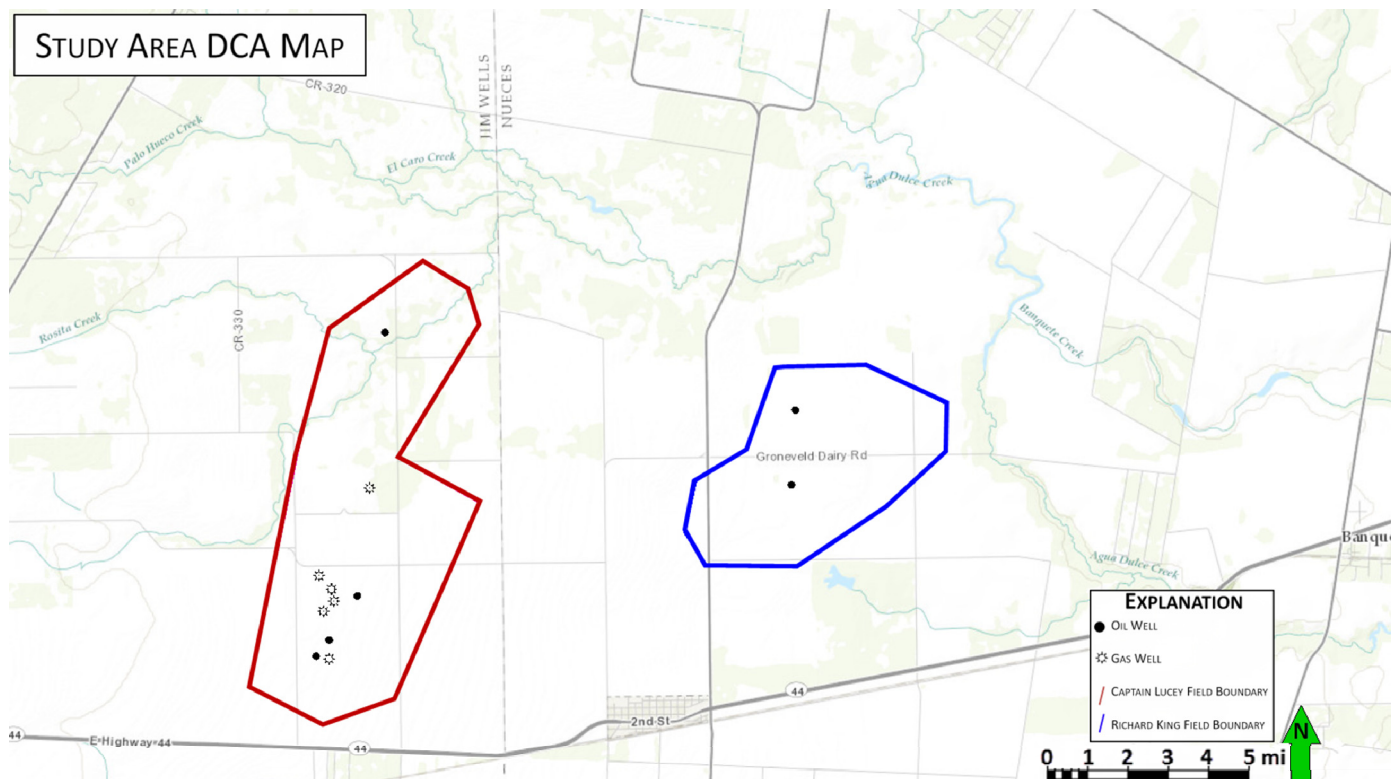


Figure 18. Map showing location of the twelve wells for the decline curve analysis.

tial utility of predicting reservoir performance based upon such associations when positioned within a sequence stratigraphic framework.

CODA

When expressed with a spatial context of 3D accommodation, depositional facies and their geometries record the discernable interplay between allocyclic and autocyclic processes. For exploration, PDCA of sands within optimal parasequence sets provides further insight and potential predictive merit into determining how such reservoirs will behave under production. For development, if augmented with 3D seismic and modeled with petroleum engineering hydrologic flow units, PDCA can potentially provide an incentive for the re-examination of mature fields for by-passed pay and new opportunities.

ACKNOWLEDGMENTS

We are indebted to Quatro Oil & Gas, Inc. and especially to John Bradley for providing access to its extensive data for this study. We also are grateful for the assistance of Corky Cummings with the PDCA of the Quatro wells. We also thank Schlumberger for furnishing its Petrel software to the Conoco-Phillips School of Geology & Geophysics for our petrophysical analysis. We acknowledge the constructive reviews of W. B. Clopine, R. D. Neese, and R. P. Major, which greatly improved an early draft of the manuscript. JDP is especially appreciative for insight into differing perspectives of the autocyclic-allocyclic polemic provided in the classrooms of the University of Texas through the didactics of W. L. Fisher, L. Frank Brown, and A. J. Scott, later at Northwestern University with L. L. Sloss, and finally in the applied laboratory of Amoco International with Brian Barrick, Martin Cassidy, and Bud Hampton.

REFERENCES CITED

- Akers, W. H., and C. W. Drooger, 1957, Miogypsinids, planktonic foraminifera, and Gulf Coast Oligocene-Miocene correlations: *American Association of Petroleum Geologists Bulletin*, v. 41, p. 656–678.
- Arps, J. J., 1945, Analysis of decline curves: *American Institute of Mechanical Engineers Transactions*, v. 160, p. 228–247.
- Beerbower, J. R., 1964, Cyclothems and cyclic depositional mechanisms in alluvial plain sedimentation, in D. F. Merriam, ed., *Symposium on cyclic sedimentation: Kansas Geological Survey Bulletin* 169, Lawrence, p. 31–42.
- Catuneanu, O. V., 2007, *Principles of sequence stratigraphy*: Elsevier, New York, New York, 375 p.
- Catuneanu, O. V., V. Abreu, J. P. Bhattacharya, M. D. Blum, R. W. Dalrymple, P. G. Eriksson, C. R. Fielding, W. L. Fisher, W. E. Galloway, M. R. Gibling, K. A. Giles, J. M. Holbrook, R. Jordan, C. G. St. C. Kendall, B. Macurda, R. Martinsen, A. D. Miall, J. E. Neal, D. Nummedal, L. Pomar, H. W. Posamentier, B. R. Pratt, J. F. Sarg, K. W. Shanley, R. J. Steel, A. Strasser, M. E. Tucker, and C. Winker, 2009, Towards the standardization of sequence stratigraphy: *Earth-Science Reviews*, v. 92, p. 1–33.
- Christie-Blick, N., and N. W. Driscoll, 1995, Sequence stratigraphy: *Annual Reviews of Earth and Planetary Sciences*, v. 23, p. 451–478.
- Curray, J. R., 1964, Transgressions and regressions, in R. L. Miller, ed., *Marine geology*: Macmillan, New York, New York, p. 175–203.
- Duncan, E. A., 1983, Delineation of delta types, Norias Delta system, Frio Formation, South Texas: Master's Thesis, University of Texas, Austin, p. 67–67.
- Fetkovich, M. J., E. J. Fetkovich, and M. D. Fetkovich, 1996, Useful concepts for decline curve forecasting, reserve estimation, and analysis: *Society of Petroleum Engineers Reservoir Engineering*, v. 11, p. 13–22.
- Fisher, W. L., 1969, Facies characterization of Gulf Coast Basin delta systems, with some Holocene analogues: *Gulf Coast Association of Geological Societies Transactions*, v. 19, p. 239–261.
- Foster, G. W., 2012, Decline curve analysis and diagnostic methods for performance forecasting: PetroSkills, LLC, Tulsa, Oklahoma, 220 p.
- Galloway, W. E., 1989, Genetic stratigraphic sequences in basin analysis; I, Architecture and genesis of flooding–surface bounded depositional units: *American Association of Petroleum Geologists Bulletin*, v. 73, p. 125–142.
- Galloway, W. E., and D. K. Hobday, 1983, Terrigenous clastic depositional systems; applications to petroleum, coal and uranium exploration: Springer Verlag, Berlin, Germany, p. 438–438.
- Galloway, W. E., D. K. Hobday, and K. Magara, 1982, Frio Formation of the Texas Gulf Coast Basin; depositional systems, structural framework, and hydrocarbon origin, migration, distribution, and exploration potential: *Texas Bureau of Economic Geology Report of Investigations* 122, Austin, 78 p.
- Haq, B. U., and A. M. Al-Qahtani, 2005, Phanerozoic cycles of sea-level change on the Arabian Platform: *GeoArabia*, v. 10, p. 127–160.
- Holtz, M. H., and L. E. McRae, 1995, Identification and assessment of remaining oil resources in the Frio fluvial-deltaic sandstone play, South Texas: *Texas Bureau of Economic Geology Report of Investigations* 227, 57 p.
- Jervey, M. T., 1988, Quantitative geological modeling of siliciclastic rock sequences and their seismic expression, in C. K. Wilgus, B. S. Hasting, C. Kendall, H. W. Posamentier, C. A. Ross, and J. C. Van Wagoner, eds., *Sea-level changes: An integrated approach*: Tulsa, Oklahoma: Society of Economic Paleontologists and Mineralogists Special Publication 42, Tulsa, Oklahoma, p. 47–69.
- Lawless, P. N., R. H. Fillon, and R. G. Lytton, III, 1997, Gulf of Mexico Cenozoic biostratigraphic, lithostratigraphic, and sequence stratigraphic event chronology: *Gulf Coast Association of Geological Societies Transactions*, v. 47, p. 271–282.
- Miall, A. D., 2010, *The geology of stratigraphic sequences*, 2nd ed.: Springer, New York, New York, 522 p.
- Mitchum, R. M., Jr., 1977, Seismic stratigraphy and global changes of sea level, part 1: Glossary of terms used in seismic stratigraphy, in C. E. Payton, ed., *Seismic stratigraphy: Applications to hydrocarbon exploration*: American Association of Petroleum Geologists Memoir 26, Tulsa, Oklahoma, p. 205–212.
- Payton, C. E., 1977, *Seismic stratigraphy: Applications to hydrocarbon exploration*: American Association of Petroleum Geologists Memoir 26, Tulsa, Oklahoma, 516 p.
- Pigott, J. D., R. Zhai, L. K. Pigott, and T. Tonianse, 2012, Searching for the missing link: The regressive systems tract—Seismic stratigraphic evidence from the southern Gulf of Thailand: *International Petroleum Technology Conference*, Bangkok, Thailand, IPTC 1511-PP, 21 p.
- Pigott, J. D., and M. I. Abdel-Fattah, 2014, Seismic stratigraphy of the Messinian Nile Delta coastal plain: Recognition of the fluvial regressive systems tract and its potential for hydrocarbon exploration: *Journal of African Earth Sciences*, v. 95, p. 9–21.
- Pigott, J. D., and D. Radivojevic, 2010, Seismic stratigraphic based chronostratigraphy (SSBC) of the Serbian Banat region of the Basin (Pannonian Basin): *Central European Journal of Geosciences*, v. 2, p. 481–500.
- Poston, S. W., and B. D. Poe, Jr., 2008, Analysis of production decline curves: *Society of Petroleum Engineers*, Richardson, Texas, 158 p.
- Sloss, L. L., 1963, Sequences in the cratonic interior of North America: *Geological Society of America Bulletin*, v. 74, p. 93–114.
- Swanson, S. M., A. W. Karlsen, and P. D. Warwick, 2007, USGS assessment of undiscovered oil and gas resources for the Oligocene Frio and Anahuac formations, U.S. Gulf of Mexico Coastal Plain and state waters; review of assessment units, in L. Kennan, J. Pindell, and N. C. Rosen, eds., *The Paleogene of the Gulf of Mexico and Caribbean basins: Processes, events, and petroleum systems*: Proceedings of the 27th Annual Gulf Coast Section of the Society of Economic Paleontologists and

Production Decline Curve

Well: F.L. Blundell B-1
T.D. 5271'

Perf Zone: 3428-3433'
Dep. Environment: Barrier Island

Cum Gas: 598 MMCF
Cum Oil: 0 MBBL

q= 100 (5/27/1975), d= 0.09, b= 1; K= 6.99 mD, DA= 251 Ac

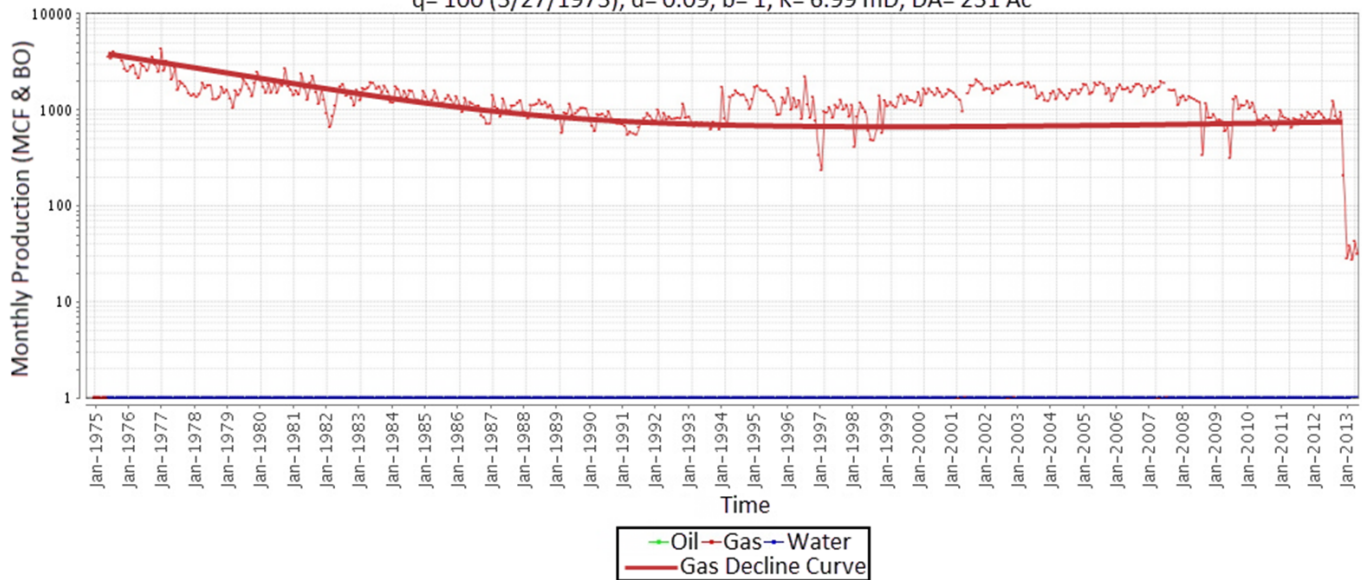


Figure 19A. Production decline curve for the F. L. Blundell B-1 well (production data courtesy of DrillingInfo, Inc.). This production decline curve is representative of the decline curve for barrier island gas reservoirs in the study area.

Production Decline Curve

Well: F.L. Blundell 7
T.D. 6252'

Perf Zone: 5899-5904'
Dep. Environment: Delta Front

Cum Gas: 176 MMCF
Cum Oil: 127 MBBL

q= 32 (11/18/1983), d= 0.09, b= 0.05; K= 45.2 mD, DA= 483 Ac

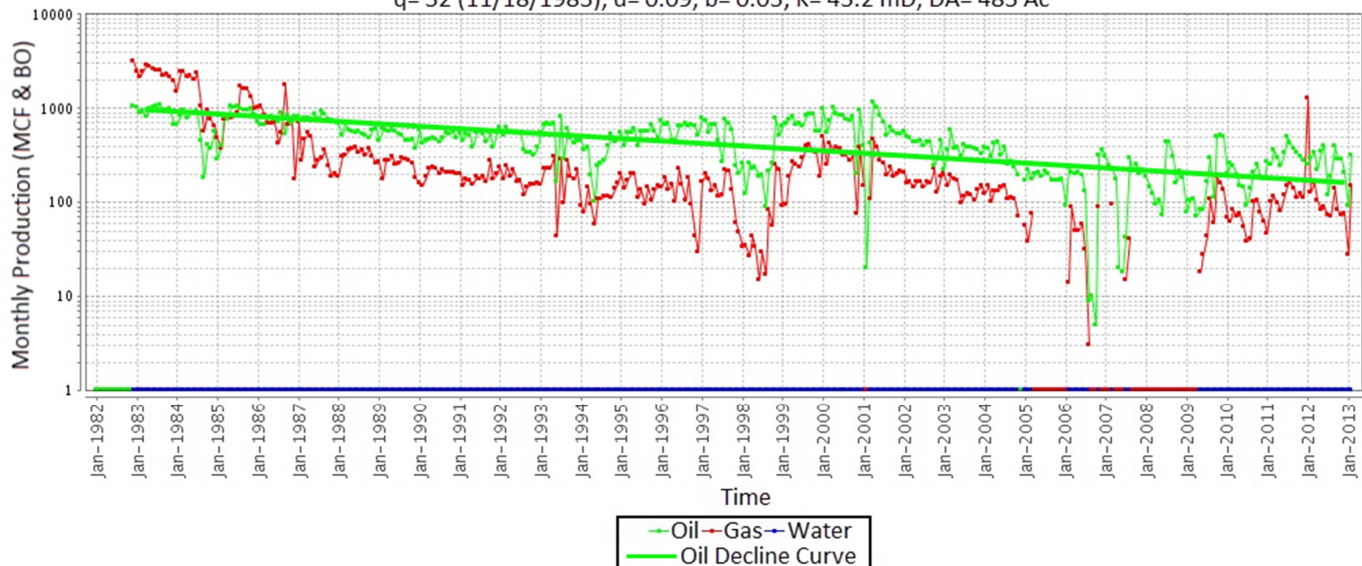


Figure 19B. Production decline curve for the F. L. Blundell 7 well (production data courtesy of DrillingInfo, Inc.). This production decline curve is representative of the decline curve for deltaic oil reservoirs in the study area.

Production Decline Curve

Well: Moore 1 Perf Zone: 3771-3777' Cum Gas: 586 MMCF
 T.D. 6002' Dep. Environment: Fluvial Channel Cum Oil: 0.05 MBBL
 $q = 415$ (8/6/1993), $d = 0.23$, $b = 0$; $K = 3.69$ mD, $DA = 386$ Ac

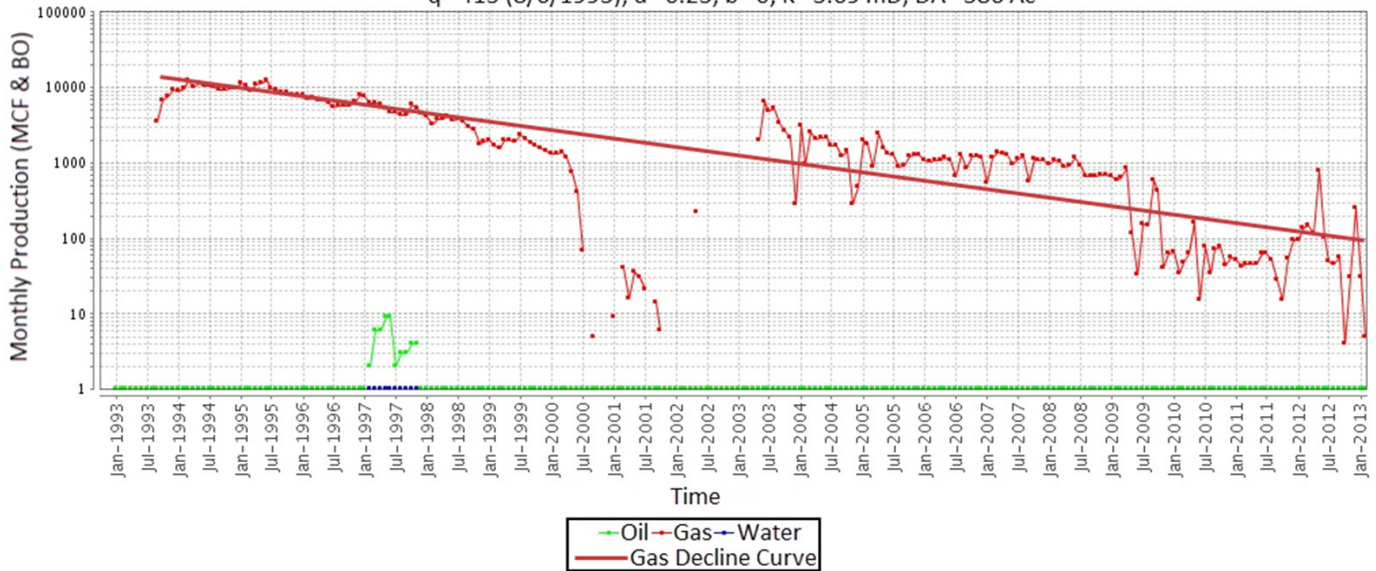


Figure 19C. Production decline curve for the Moore 1 well (production data courtesy of DrillingInfo, Inc.). This production decline curve is representative of the decline curve for fluvial channel gas reservoirs in the study area.

Production Decline Curve

Well: Walker A-4 Perf Zone: 5425-5430' Cum Gas: 28.3 MMCF
 T.D. 6444' Dep. Environment: Fluvial Channel Cum Oil: 5.2 MBBL
 $q = 140$ (12/5/1976), $d = 0.66$, $b = 0.5$; $K = 55.3$ mD, $DA = 167$ Ac

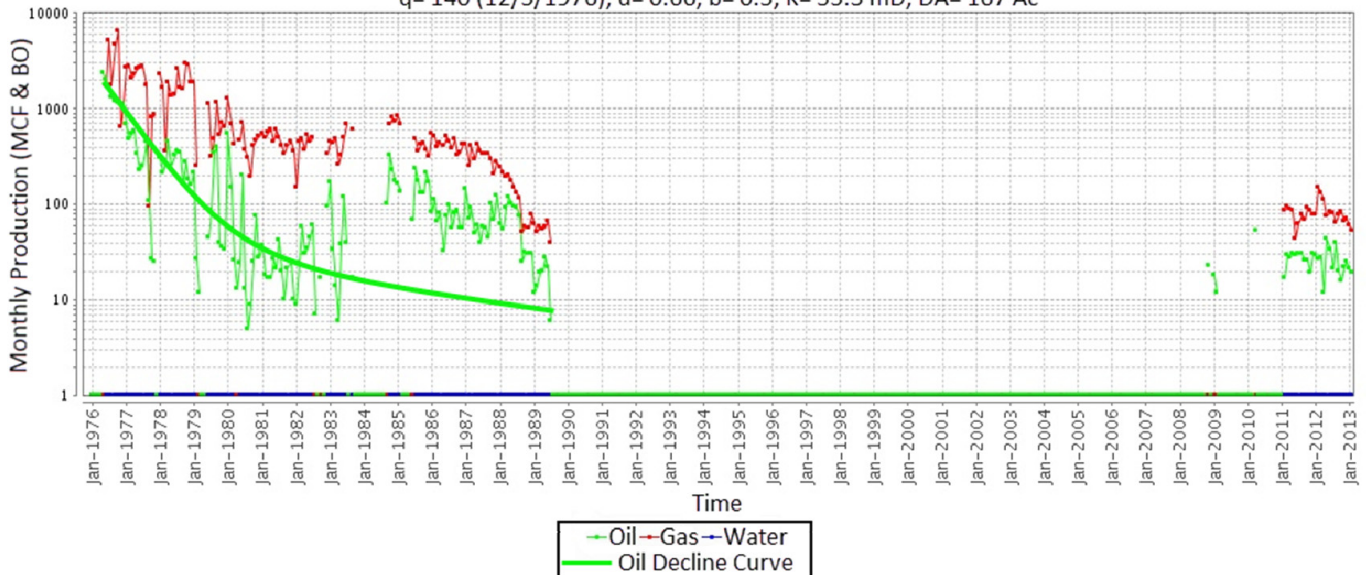


Figure 19D. Production decline curve for the Walker A-4 well (production data courtesy of DrillingInfo, Inc.). This production decline curve is representative of the decline curve for fluvial channel oil reservoirs in the study area.

Production Decline Curve

Well: F.L. Blundell 8
T.D. 6180'

Perf Zone: 3774-3779'
Dep. Environment: Crevasse-Splay

Cum Gas: 35.6 MMCF
Cum Oil: 0 MBBL

$q = 38 (1/5/1994), d = 0.34, b = 0; K = 0.88 \text{ mD}, DA = 109 \text{ Ac}$

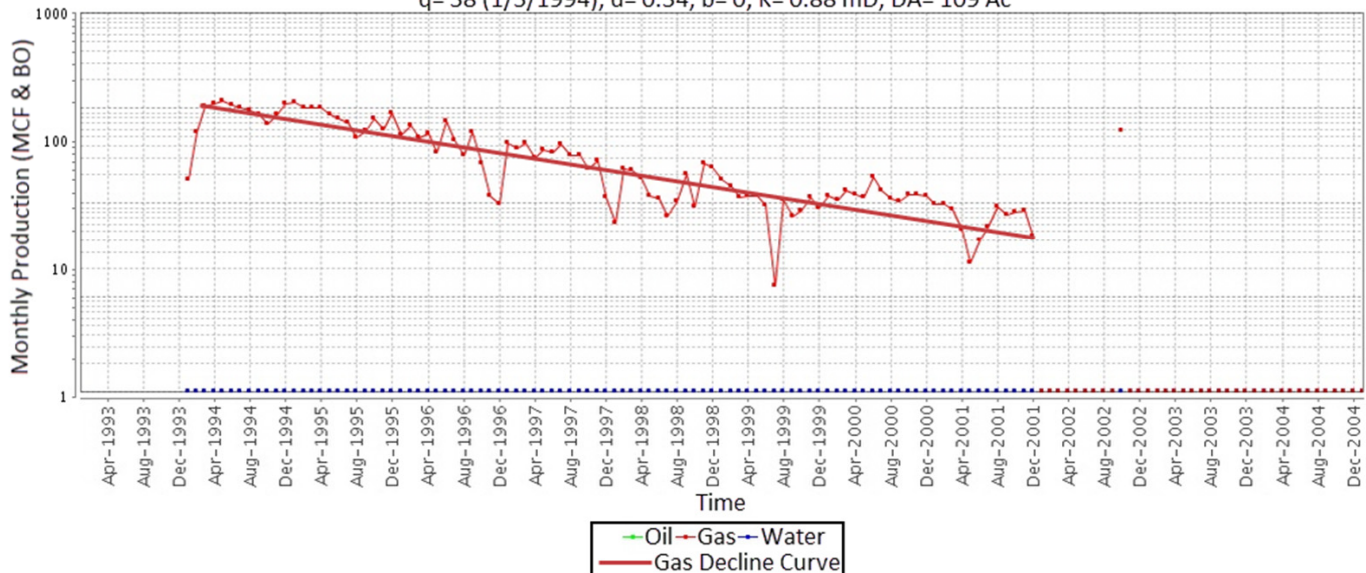


Figure 19E. Production decline curve for the F. L. Blundell 8 well (production data courtesy of DrillingInfo, Inc.). This production decline curve is representative of the decline curve for crevasse-splay gas reservoirs in the study area.

Table 1. Reservoir log-derived porosity and PDCA output for 18 Frio reservoirs of Captain Lucy and Richard King fields. See text for description and discussion of variables.

Depositional Environment	Average Porosity (%)	Gas					Oil					Cumulative				
		q_i	D_i	B	k (mD)	DA (ac)	q_i	D_i	B	k (mD)	DA (ac)	q_i	D_i	B	k (mD)	DA (ac)
Fluvial Channel	24	241.5	0.27	0.033	2.85	214	47	0.44	0.421	57.28	213	111.5	0.12	0.015	32.16	214
		n=12					n=8					n=20				
Deltaic	22						66.25	0.37	0.238	80.13	291	66.25	0.37	0.238	80.13	291
		n=1					n=2					n=20				
Crevasse Splay	20	38	0.34	0	0.83	109						38	0.34	0	0.83	109
		n=1										n=1				
Barrier Island	25	100	0.09	1	6.98	251						100	0.09	1	6.98	251
		n=1										n=1				

Mineralogists Foundation Bob F. Perkins Research Conference, Houston, Texas, p. 341–375.

Vail, P. R., R. M. Mitchum, Jr., and S. Thompson, III, 1977, Seismic stratigraphy and global changes of sea level; part 3, relative changes of sea level from coastal onlap, in C. E. Payton, ed., Seismic stratigraphy: Applications to hydrocarbon exploration: American Association of Petroleum Geologists Memoir 26, Tulsa, Oklahoma, p. 63–81.

Van Wagoner, J. C., R. M. Mitchum, K. M. Campion, and V. D. Rahmanian, 1990, Siliciclastic sequence stratigraphy in well logs, cores, and outcrops; concepts for high-resolution correla-

tion of time and facies: American Association of Petroleum Geologists Methods in Exploration Series 7, Tulsa, Oklahoma, 55 p.

Wilgus, C. K., B. S. Hasting, C. G. St. C. Kendall, H. W. Posamentier, C. A. Ross, and J. C. Van Wagoner, eds., 1988, Sea-level changes; an integrated approach: Society of Economic Paleontologists and Mineralogists Special Publication 42, Tulsa, Oklahoma, 407 p.

Wright, V. P., and S. B. Marriott, 1993, The sequence stratigraphy of fluvial depositional systems: The role of floodplain sediment storage: Sedimentary Geology, v. 86, p. 203–210.